Department of Mechanical Engineering

Driving Cycle Uncertainty and Energy Consumption of City Buses: Analysis and Optimization

Klaus Kivekäs

Aalto University

DOCTORAL DISSERTATIONS

Aalto University publication series
DOCTORAL DISSERTATIONS 133/2019

Driving Cycle Uncertainty and Energy Consumption of City Buses: Analysis and Optimization

Klaus Kivekäs

A doctoral dissertation completed for the degree of Doctor of Science (Technology) to be defended, with the permission of the Aalto University School of Engineering, at a public examination held at the lecture hall K1/216 of the school on 23 August 2019 at 12:00.

Aalto University
School of Engineering
Department of Mechanical Engineering
Engineering Design

Supervising professors
Associate Professor Kari Tammi
Aalto University
Finland

Preliminary examiners
Associate Professor Theo Hofman
Eindhoven University of Technology
The Netherlands

Associate Professor Reza Ghabcheloo
Tampere University of Technology
Finland

Opponents
Associate Professor Theo Hofman
Eindhoven University of Technology
The Netherlands

Aalto University publication series
DOCTORAL DISSERTATIONS 133/2019

ISBN 978-952-60-8647-7 (printed)
ISBN 978-952-60-8648-4 (pdf)
ISSN 1799-4934 (printed)
ISSN 1799-4942 (pdf)
http://urn.fi/URN:ISBN:978-952-60-8648-4

Unigrafia Oy
Helsinki 2019

Finland

Printed matter
4041-0619

Aalto University

Abstract

Aalto University, P.O. Box 11000, FI-00076 Aalto www.aalto.fi

Author
Klaus Kivekäs

Name of the doctoral dissertation
Driving Cycle Uncertainty and Energy Consumption of City Buses: Analysis and Optimization

Publisher School of Engineering

Unit Department of Mechanical Engineering

Series Aalto University publication series DOCTORAL DISSERTATIONS 133/2019

Field of research Engineering Design

Manuscript submitted 24 April 2019 **Date of the defence** 23 August 2019

Permission for public defence granted (date) 25 June 2019 **Language** English

☐ **Monograph** ☒ **Article dissertation** ☐ **Essay dissertation**

Abstract

The research presented here studied the effect of driving cycle variation and passenger load uncertainty on the energy consumption of city buses. Furthermore, different methods for reducing the energy consumption were analyzed and compared. The research was conducted with simulation studies. In order to generate a large quantity of varying realistic cycles for a single bus route, a novel driving cycle synthetization algorithm was developed. The algorithm is capable of synthesizing a large number of cycles based on only a handful of measurements by exploring different combinations of events. Cycles generated with the algorithm were employed to compare the energy consumption of different city bus powertrain topologies under uncertainty in the driving cycle and passenger load. Simulated bus powertrain topologies included: compressed natural gas, diesel, parallel hybrid, series hybrid, hydrogen fuel cell hybrid, and battery electric bus.

Synthetic driving cycles generated with the novel cycle synthesis algorithm were shown to maintain the statistical properties of the original measured cycles with good accuracy. The presented algorithm could be utilized to further optimize city buses for the routes they will be operated on. Energy consumption results acquired from the simulation studies indicated that battery electric buses are the most robust option against driving cycle uncertainty. Diesel buses appeared to be the most sensitive to the driving aggressiveness. However, the results displayed a strong correlation between energy consumption and driving aggressiveness with all types of powertrains. This suggests that steps should be taken to limit high-speed accelerations of city buses regardless of powertrain type.

Battery electric buses were further studied by comparing component-choice-related methods for reducing the energy consumption. The methods included using an aluminum chassis instead of a steel chassis, employing a low-height body for reduced aerodynamic drag, using low-rolling-resistance class C tires, and utilizing an electric heat pump instead of a more conventional electric heater. A novel problem formulation for driving optimization was devised for a nonlinear model predictive controller. The driving optimization algorithm was used to compare the energy savings achievable with predictive driving to those achieved with the component-choice-related methods.

Out of all the considered consumption reduction methods, the heat pump produced the highest energy savings in cold conditions. However, the relative effectiveness of the heat pump was significantly influenced by the ambient temperature and driving cycle. The aluminum chassis provided higher consumption reductions than the low-rolling-resistance tires, but the influence of the lighter chassis was highly dependent on the aggressiveness of the driving. On average, the predictive driving achieved higher energy savings than the aluminum chassis. Applying all of the methods simultaneously resulted in an average consumption reduction of more than 30 %.

Keywords city bus, driving cycle, energy consumption, passenger load, powertrain, predictive control, uncertainty

ISBN (printed) 978-952-60-8647-7 **ISBN (pdf)** 978-952-60-8648-4

ISSN (printed) 1799-4934 **ISSN (pdf)** 1799-4942

Location of publisher Helsinki **Location of printing** Helsinki **Year** 2019

Pages 139 **urn** http://urn.fi/URN:ISBN:978-952-60-8648-4

Aalto-yliopisto

Tiivistelmä

Aalto-yliopisto, PL 11000, 00076 Aalto www.aalto.fi

Tekijä
Klaus Kivekäs

Väitöskirjan nimi
Ajosyklin epävarmuus ja kaupunkibussien energiankulutus: analyysi ja optimointi

Julkaisija Insinööritieteiden korkeakoulu

Yksikkö Konetekniikan laitos

Sarja Aalto University publication series DOCTORAL DISSERTATIONS 133/2019

Tutkimusala Insinöörisuunnittelu

Käsikirjoituksen pvm 24.04.2019 **Väitöspäivä** 23.08.2019

Väittelyluvan myöntämispäivä 25.06.2019 **Kieli** Englanti

☐ **Monografia** ☒ **Artikkeliväitöskirja** ☐ **Esseeväitöskirja**

Tiivistelmä

Tutkimuksessa selvitettiin perusteellisesti ajosyklin vaihteluiden ja matkustajakuorman epävarmuuden vaikutusta kaupunkibussien energiankulutukseen. Lisäksi tutkittiin metodeja energiankulutuksen vähentämiseksi. Tutkimus toteutettiin simulaatioiden avulla. Uusi ajosyklien syntetisointialgoritmi kehitettiin, jotta pystyttäisiin generoimaan suuri määrä vaihtelevia realistisia syklejä tietylle bussireitille. Algoritmi kykenee syntetisoimaan suuren määrän syklejä pienen mittadatajoukon perusteella käyttämällä erilaisia tapahtumien kombinaatioita. Synteesialgoritmin avulla vertailtiin, kuinka ajosykli- ja matkustajakuormaepävarmuus vaikuttavat energiankulutukseen erilaisilla käyttövoimajärjestelmän topologioilla. Seuraavia kaupunkibussien käyttövoimajärjestelmiä vertailtiin simulaatioissa: paineistettu maakaasu, diesel, rinnakkais- ja sarjahybridi, vetypolttokennohybridi sekä täyssähkö.

Tulokset osoittivat, että syklisynteesialgoritmi kykenee tuottamissaan sykleissä säilyttämään alkuperäisten mitattujen syklien tilastolliset ominaisuudet tarkasti. Tällaista syklisynteesiä olisi mahdollista käyttää esimerkiksi optimoimaan kaupunkibusseja paremmin niille reiteille, joilla niitä tiedetään tultavan käyttämään. Energiankulutustutkimusten tulokset osoittivat, että sähköbussit ovat robusteimpia ajosykliepävarmuutta vastaan. Dieselbussit puolestaan osoittautuivat kaikista herkimmiksi ajotyylin aggressiivisuudelle. Tuloksista kuitenkin myös havaittiin energiankulutuksen korreloivan voimakkaasti ajotyylin aggressiivisuuden kanssa kaikenlaisilla käyttövoimajärjestelmän konfiguraatioilla. Tämä tulos kertoo, että olisi erityisen tärkeää rajoittaa kaupunkibussien kiihtyvyyksiä korkeissa nopeuksissa riippumatta bussin käyttövoimajärjestelmästä.

Bussien komponentteihin liittyviä energiankulutuksen vähentämisen metodeja vertailtiin sähköbussin tapauksessa. Metodeihin kuului kevyen alumiinirungon käyttäminen teräksisen rungon sijaan, matalan koriprofiilin käyttö ilmanvastuksen pienentämiseksi, pienemmän vierimisvastuksen omaavien C-luokan renkaiden käyttäminen ja sähköisen lämpöpumpun käyttö perinteisen sähkölämmittimen sijaan. Epälineaariselle mallipohjaiselle ennakoivalle kontrollerille luotiin uudenlainen ajo-optimoinnin ongelman muotoilu. Ajo-optimointialgoritmia käytettiin vertailemaan ennakoivalla ajolla saavutettavia energiasäästöjä aiemmin mainittujen metodien tuottamiin säästöihin.

Lämpöpumppu tuotti suurimmat energiasäästöt vertailluista metodeista kylmissä ulkoilmaolosuhteissa. Lämpöpumpun kyky vähentää energiankulutusta suhteessa muihin metodeihin riippui kuitenkin voimakkaasti ulkoilman lämpötilasta sekä ajosyklin tyypistä. Alumiinirunko vähensi kulutusta enemmän kuin C-luokan renkaiden käyttäminen, mutta kevyemmän rungon vaikutus riippui merkittävästi ajotyylin aggressiivisuudesta. Ennakoiva ajo tuotti keskimäärin suuremmat energiasäästöt kuin alumiininen runko. Kun kaikkia metodeja käytettiin yhtä aikaa, väheni bussin energiankulutus keskimäärin yli 30 %.

Avainsanat ajosykli, energiankulutus, ennakoiva ohjaus, epävarmuus, kaupunkibussi, käyttövoimajärjestelmä, matkustajakuorma

ISBN (painettu) 978-952-60-8647-7 **ISBN (pdf)** 978-952-60-8648-4

ISSN (painettu) 1799-4934 **ISSN (pdf)** 1799-4942

Julkaisupaikka Helsinki **Painopaikka** Helsinki **Vuosi** 2019

Sivumäärä 139 **urn** http://urn.fi/URN:ISBN:978-952-60-8648-4

Preface

This thesis is based on research carried out in the research group led by Professor Kari Tammi. I would like to thank Professor Tammi, who acted as the instructor and supervisor for the thesis work, for the tremendous amount of inspiration and guidance he provided throughout my studies. Without his help and patient encouragement, the completion of this thesis would not have been possible.

I would also like to extend my gratitude to all the colleagues I got to work with during these years. I wish to thank Professor Antti Lajunen for all the assistance and resources he provided. His input was immensely important to the completion of the second and third publications. I would also like to thank my fellow doctoral student Jari Vepsäläinen, who contributed significantly to my research work. His input was invaluable in devising the different research topics as well as in the development of the simulation models and the implementation of the different statistical analysis methods used in this research. His positive attitude also helped to encourage me to get through the difficult periods during the studies. The contributions of Dr. Francesco Baldi to the third publication are also greatly appreciated. Furthermore, I would like to thank Risto Ojala for his help in proofreading and improving the language of my publications and thesis.

In addition, I would like to thank the crew at the *pöhinäparveke*, including Janne, Jari, Jesse, Risto, and Antti, as well as all the rest of my colleagues working in the research groups of Professor Petri Kuosmanen and Professor Kari Tammi for creating a cheerful and enjoyable work environment.

I am also grateful for the funding from Business Finland, Yrjö and Senja Koivunen Foundation, Henry Ford Foundation Finland, and Volvo Foundation for Bus Traffic, Finland. Furthermore, I wish to thank Sami Ruotsalainen and Linkker for providing us with large amounts of data from electric buses for the research. Additionally, I am thankful to Petri Söderena and VTT Technical Research Centre of Finland for supplying diesel bus measurement data.

Professor Theo Hofman from Eindhoven University of Technology and Professor Reza Ghabcheloo from Tampere University of Technology are greatly acknowledged for pre-examining this dissertation.

Finally, I would like to thank my family for being so understanding and supportive throughout my studies.

Espoo, 29 June 2019
Klaus Vilhelm Kivekäs

Contents

List of Abbreviations and Symbols

a	Acceleration
A	Vehicle frontal area
AC	Air conditioning
AUX	Auxiliary devices
B18	Berkeley bus line 18
B51	Berkeley bus line 51
BAT	Battery
BEB	Battery electric bus
BR	Braunschweig
c_D	Aerodynamic drag coefficient
C_b	Battery capacity (in ampere hours)
C_τ	Capacitance of the capacitor in a Thévenin battery model
CNG	Compressed natural gas
d_c	Total distance of the driving cycle
dq	Direct-quadrature
DP	Dynamic programming
e_s	Slack variable
E	Energy consumption
E11	Espoo bus line 11
E11B	Espoo bus line 11 alternative driving cycle
EM	Electric motor
EV	Electric vehicle
F_B	Mechanical braking force

$F_{B,max}$	Maximum negative mechanical braking force
F_d	Aerodynamic drag force
F_G	Gravitational force
F_{rr}	Rolling resistance force
F_R	Total resistive force
F_w	Tractive force
FC	Fuel cell
FCH	Fuel cell hybrid
FD	Final drive
g	Standard acceleration due to gravity
GB	Gearbox
GC	Generator and controller
GHG	Greenhouse gas
GPS	Global Positioning System
GSA	Global Sensitivity Analysis
H1	Helsinki 1 city bus test driving cycle
H2	Helsinki 2 city bus test driving cycle
H24	Helsinki bus line 24
H3	Helsinki 3 city bus test driving cycle
H55	Helsinki bus line 55
H550	Helsinki bus line 550
H58	Helsinki bus line 58
HSL	Helsinki Regional Transport Authority
HVAC	Heating, ventilation, and air conditioning
i_b	Battery current
i_d	Stator d-axis current
i_{fd}	Final drive gear ratio
i_g	Gearbox gear ratio
i_{max}	Electric motor maximum current
i_q	Stator q-axis current

i_s	Electric motor stator current
ICE	Internal combustion engine
IoT	Internet of things
J_t	Total moment of inertia superimposed at the driven axle
k	Discrete time instant
L_s	Electric motor stator inductance
L05	Lahti bus line 05
L31	Lahti bus line 31
m	Total mass of the vehicle
MAN	Manhattan driving cycle
MC	Electric motor and controller
MLE	Maximum likelihood estimation
MLR	Multiple linear regression
MPC	Model predictive control
NMPC	Nonlinear model predictive control
NYC	New York City driving cycle
OCC	Orange County driving cycle
P_{aux}	Auxiliary device power demand
$P_{EM,in}$	Electric motor input power
$P_{EM,max}$	Maximum electric motor output power
$P_{EM,min}$	Minimum electric motor output power
$P_{EM.out}$	Electric motor output power
P_s	Electric motor input power (in the space-vector model)
PCA	Principal component analysis
PMSM	Permanent magnet synchronous motor
p	Number of pole pairs in an electric motor
q_b	State-of-charge of the battery
QP	Quadratic programming
r^2	Coefficient of determination
r_d	Wheel dynamic radius

R_{int}	Battery internal resistance
R_s	Electric motor stator resistance
R_{ss}	Resistance of the steady-state resistance component in a Thévenin battery model
R_τ	Resistance of the transient resistance component in a Thévenin battery model
R36	Nuremberg route R36 driving cycle
RMSE	Root-mean-square error
RTE	Denver Regional Transportation District city bus driving cycle
s	Laplace-domain variable
SOC	State-of-charge
SQP	Sequential quadratic programming
SSE	Sum of squares of residuals
SST	Total sum of squares
t	Time
T_{EM}	Electric motor torque
$T_{EM,max}$	Maximum electric motor torque
$T_{EM,min}$	Minimum electric motor torque
$T_{EM,req}$	Electric motor torque requested by the controller
T_s	Controller sample time
TA25	Tampere bus line 25 driving cycle
TC	Torque coupler
TU03	Turku bus line 03 driving cycle
u_1	First control variable in a state-space model
u_2	Second control variable in a state-space model
u_b	Battery output voltage
$u_{C\tau}$	Voltage over the capacitor in a Thévenin battery model
u_{max}	Electric motor maximum voltage
u_{oc}	Battery open-circuit voltage
$u_{R\tau}$	Voltage over the transient resistance component in a Thévenin battery model
u_s	Electric motor stator voltage

v	Speed
v_{max}	Maximum speed
$\hat{V}_i$	Total contribution of an input variable to the variance of an output variable
$\hat{V}_i^C$	Contribution of an input variable to the variance of an output variable that is correlated with the contributions of other input variables
$\hat{V}_i^U$	Contribution of an input variable to the variance of an output variable that is not correlated with the contributions of other input variables
x_1	First state in a state-space model
x_2	Second state in a state-space model
X_p	Average number of passengers in the bus during a cycle
X_s	Number of stops at bus stops during a cycle
α	Road grade
η_{EM}	Combined efficiency of the electric motor and inverter
η_{fd}	Final drive efficiency
η_g	Gearbox efficiency
η_i	Inverter efficiency
$\eta_{m\prime}$	Approximated combined efficiency of the electric motor and inverter
$\eta_{m,c}$	Approximated constant value for the combined efficiency of the electric motor and inverter
H_{dt}	Drivetrain efficiency variable
$H_{dt,2}$	Drivetrain efficiency variable used in the NMPC algorithm
$H_{m\prime}$	Variable representing an approximation of the combined efficiency of the electric motor and inverter in the cost function of the NMPC driving optimization algorithm
μ_p	Overall average number of passengers in the bus during measured cycles
μ_s	Average number of stops at bus stops during measured driving cycles
ρ	Density of air
ρ_{ps}	Pearson correlation coefficient for mean number of passengers in the bus and stops performed at bus stops during a cycle in measured cycles

ρ_{xy}	Pearson correlation coefficient for variables x and y
σ_i	Standard deviation of variable i
σ_p	Standard deviation of average number of passengers in the bus during a cycle in measured cycles
σ_s	Standard deviation of number of stops at bus stops during a driving cycle in measured cycles
τ	Time response of electric motor
ψ_f	Permanent flux induced by magnets
ψ_s	Electric motor stator flux linkage
ω_{EM}	Electric motor rotational speed
ω_m	Electric motor electrical angular speed

List of Publications

This doctoral dissertation consists of a summary and of the following publications which are referred to in the text by their numerals.

I. Kivekäs, Klaus; Vepsäläinen, Jari; Tammi, Kari. 2018. Stochastic Driving Cycle Synthesis for Analyzing the Energy Consumption of a Battery Electric Bus. IEEE. IEEE Access, 6, pages 55586-55598. 2169-3536. https://doi.org/10.1109/ACCESS.2018.2871574

II. Kivekäs, Klaus; Lajunen, Antti; Vepsäläinen, Jari; Tammi, Kari. 2018. City Bus Powertrain Comparison: Driving Cycle Variation and Passenger Load Sensitivity Analysis. MDPI. MDPI Energies, 11, 7. 1996-1073. https://doi.org/10.3390/en11071755

III. Kivekäs, Klaus; Lajunen, Antti; Baldi, Francesco; Vepsäläinen, Jari; Tammi, Kari. Reducing the Energy Consumption of Electric Buses with Design Choices and Predictive Driving. IEEE. Accepted for publication in the journal IEEE Transactions on Vehicular Technology in April 2019.

Author's Contribution

Publication I: Stochastic Driving Cycle Synthesis for Analyzing the Energy Consumption of a Battery Electric Bus

The author developed the stochastic driving cycle synthetization method based on previous work conducted by Joel Anttila. The author created the simulation model of an electric bus used in the study together with co-author Jari Vepsäläinen. The author prepared the simulations and parametrized and validated the simulation model. The author conducted a statistical analysis of the results in order to examine the influence of driving cycle uncertainty on the energy consumption of an electric city bus. Vepsäläinen provided the code for the Global Sensitivity Analysis. The author wrote the publication with feedback from all of the co-authors. Kari Tammi helped drafting the research problem, participated in data acquisition, and assisted in processing the data. Tammi also provided instructions for the research methods.

Publication II: City Bus Powertrain Comparison: Driving Cycle Variation and Passenger Load Sensitivity Analysis

The author developed simulation models of six different city bus types together with co-author Antti Lajunen in order to compare how different powertrain configurations respond to variations in the driving cycle and passenger load. The author validated the simulation models and prepared and conducted the simulations. The author analyzed the energy consumption of the different bus types based on the simulation results together with co-author Jari Vepsäläinen. Vepsäläinen also provided the code for the variance decomposition analysis. The author wrote the publication. Co-authors Lajunen, Vepsäläinen, and Tammi commented the manuscript and its revised versions. Lajunen and Tammi helped drafting the research problem. Tammi also participated in the data acquisition and model validation and provided instructions for the research methods and writing the paper.

Publication III: Reducing the Energy Consumption of Electric Buses with Design Choices and Predictive Driving

The author developed the simulation model of a battery electric bus used in the study. Together with co-author Antti Lajunen, the author designed the simulation tests for comparing different energy consumption reduction methods for electric city buses. The author developed the nonlinear model predictive controller (NMPC) for driving optimization. The development of the

NMPC included multiple implementation questions that had to be solved before creating a functional controller. The author conducted the simulations and analyzed the results in order to examine the effectiveness of the energy consumption reduction methods. The author wrote the article. Co-authors Lajunen, Baldi, Vepsäläinen, and Tammi provided feedback on the manuscript and its revisions. Lajunen also assisted with creating the electric bus simulation model. Baldi assisted with the theory of model predictive control. Vepsäläinen gave feedback on the methods used for analyzing the simulation results. Tammi provided assistance in drafting the research problem as well as in developing the NMPC algorithm. Tammi also instructed in writing the paper.

1. Introduction

Increasing concerns regarding climate change have led to a surge of interest in green technology in recent years. The transportation sector is estimated to cause approximately 14 % of the greenhouse gas (GHG) emissions globally [1]. In the United States of America and the European Union, transportation accounts for nearly 30 % of GHG emissions [2], [3]. Reducing the pollution caused by transportation is thus seen as an urgent objective. While the rapid shift towards hybrid electric and battery electric passenger vehicles may have been the most visible aspect of transportation electrification to the general public, city buses have also been undergoing a green transformation. Battery electric buses (BEBs) tend to not suffer from the range and recharging power limitations of electric powertrains as much as passenger vehicles. Fast-charging stations can be placed at the end stations to facilitate quickly charging the battery after each run of the route. Alternatively, the buses can be charged overnight, allowing for uninterrupted operation during the day but also requiring significantly higher battery capacity [4]. Due to the viability of electric propulsion in city bus operation, ambitious programs to move away from conventional diesel buses to fully electric bus fleets are underway across the globe. For example, the bus fleets in Amsterdam and Paris are intended to be fully electric by 2025, while Shenzhen already features a fleet consisting entirely of BEBs [5], [6]. In Finland, the Helsinki Regional Transport Authority (HSL) will deploy 30 new BEBs in the fall of 2019 with an ultimate goal of reducing the carbon dioxide emissions of public transport in the Helsinki region by 90 % compared to 2010 levels by 2025 [7]. Other large Finnish cities, including Turku and Tampere, are also planning to heavily invest in electric buses [8], [9].

However, BEBs are not the only option for reducing the energy consumption and emissions of city buses. Figure 1 shows the most common powertrain configurations for city buses. In regions where the GHG intensity of the electricity production is high, hybrid electric buses can offer higher emissions reductions than BEBs [10]. Additionally, the lifecycle costs of hybrid electric buses are currently lower than those of BEBs [11]. Hydrogen fuel cell hybrid (FCH) buses offer a longer range and faster refueling than BEBs, but there are still various hurdles to overcome before FCH technology can become a cost-effective alternative. There are issues regarding the durability and reliability of fuel cells, and the availability and sustainability of hydrogen as a fuel is still uncertain [12].

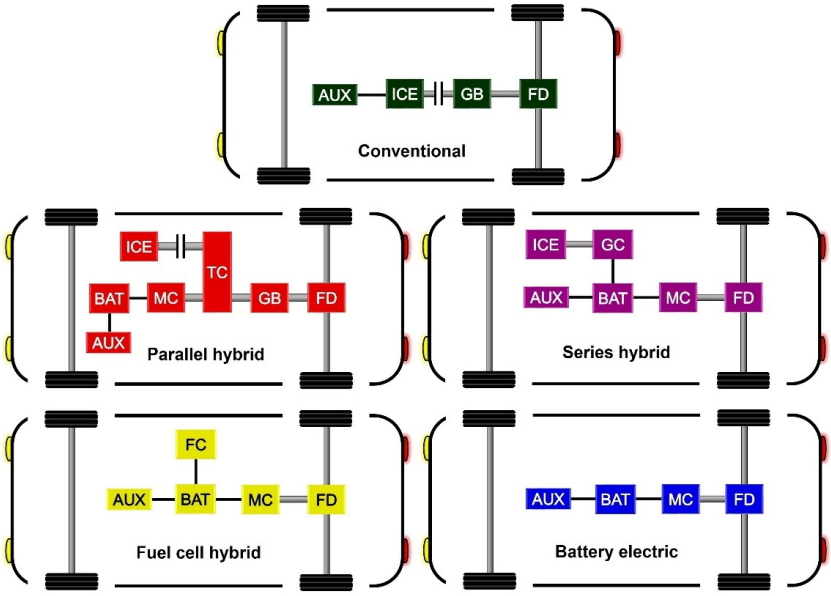

Figure 1. Simplified layouts of the most common city bus powertrain topologies (Publication II).

Several factors other than the powertrain configuration strongly influence the energy consumption and emissions of city buses. While the route of the bus is fixed, there can still be major variations in the driving cycle due to traffic, passenger demand, and driving style [13]. The term *driving cycle* means a series of data points representing the speed of a vehicle as a function of time. The passenger load is also known to have a substantial impact on the energy use [14].

As the driving route is predictable, city buses are an ideal target for autonomous driving. By optimizing the driving, the energy use can be reduced, which can be particularly beneficial in the case of electric buses due to the limited battery capacity. Furthermore, the energy consumption and emissions of city buses can be reduced with other component choices. A lightweight aluminum chassis can reduce the curb weight of the bus by approximately 15 % compared to a more conventional steel chassis [15]. Other options include a lower height body to reduce drag and low-rolling-resistance tires. Additionally, electric heat pumps are rapidly approaching the point at which they can be considered a financially viable alternative to conventional electric or diesel heaters [16]. Heat pumps provide a significantly higher thermal energy efficiency compared to the more conventional options in temperatures warmer than -20 °C [17].

1.1 Research objectives and questions

In this thesis, the energy consumption of city buses is examined with the focus being on the influence of driving cycle uncertainty, passenger load variations, and component choices as well as predictive driving. The term *uncertainty* in the context of this thesis is considered to mean variation. The following research questions are central for the thesis:

1. How can you generate a large quantity of varying realistic driving cycles and passenger loads for a single bus route based on limited measurement data?
2. How do driving cycle and passenger load variations affect the energy consumption of different city bus powertrains on a single bus route?
3. How do different driving cycle characteristics and the aggressiveness of the driving influence the energy consumption of different city bus powertrain topologies?
4. How significant energy consumption reductions can be achieved with different component-related choices with BEBs?
5. How should the driving optimization problem be formulated for a nonlinear model predictive control (NMPC) algorithm in order to minimize the energy consumption of a BEB?
6. How much can predictive driving reduce the energy consumption of a BEB?

These six research questions are answered in Publications I, II, and III. Publication I focuses on questions 1 and 2 and provides the groundwork for Publication II. Publication II tackles question 2 as well but, unlike Publication I, considers several types of city bus powertrains instead of only battery electric powertrain. Publication II also answers research question 3. Publication III provides answers for research questions 4, 5, and 6. The research in this thesis focuses on simulation studies. In Publications I and III, the simulation models were created in MATLAB and Simulink. In Publication II, the Autonomie vehicle simulation software was used. Model validation was conducted by comparing selected key outputs of the simulation models to measurement data.

1.2 Motivation

The motivation of the research is to provide new tools for forecasting the energy consumption variations on a single bus route, to provide new information about the influence of different driving cycle properties on the energy consumption of different types of city bus powertrains, and to provide new information about the effectiveness of different component-choice-related methods as well as predictive driving for reducing the energy consumption of BEBs. The ability to forecast the energy consumption variations caused by driving cycle uncertainty and passenger load variations on a specific route can benefit various parties, including the public transport authority, route operators, bus manufacturers, as well as public transport users. Powertrain dimensioning could be optimized better for the route by using simulations to forecast the energy consumption distributions. In turn, cost efficiency would be improved, particularly due to the ability to scale the battery more accurately, reducing the weight of the bus and thereby improving the energy efficiency.

Increased knowledge of how the energy consumption is influenced by different driving cycle properties and passenger load variations can help inform which types of powertrain topologies are best suited for different kinds of bus

routes. Additionally, a better grasp of the most influential driving cycle properties can improve energy consumption prediction methods and the development of autonomous driving algorithms. Furthermore, information about the effectiveness of different methods for reducing the energy consumption of BEBs can be highly significant to bus manufacturers. When weighing the different options against each other in order to reach a desired energy consumption reduction target, it is highly important to have detailed knowledge of the magnitude of the reductions that are achievable with the different methods. Examining the optimal way to formulate the driving optimization problem for an NMPC controller should also prove useful for autonomous driving algorithm development.

1.3 Scientific contribution

In previous city bus simulation studies, driving cycles from a multitude of different regions have been employed. However, the energy consumption variations on a single bus route caused by driving cycle uncertainty have not been investigated in previous works. Furthermore, while numerous driving cycle construction methods have been presented in previous publications, the methods have mainly focused on generating a single statistically representative cycle based on a large amount of measurement data. Methods for generating a large number of varying cycles for a single bus route based on limited measurement data have not been considered. These are the main research gaps that Publication I aimed to fill. In Publication I, a novel driving cycle synthetization method was presented, and it was used to generate a large quantity of driving cycles and passenger loads for a typical suburban bus route in Finland. A simulation model of a BEB created in Simulink was then employed to analyze the consumption fluctuations caused by the driving cycle uncertainty and passenger load variations.

Publication II built on the work presented in Publication I. Alternative city bus powertrain topologies have been compared from a multitude of different angles in previous publications. However, the differences between the different powertrains in the energy consumption variations caused by driving cycle uncertainty and passenger load variations have not been examined. In Publication II, this research gap was filled by using the cycle synthesis method developed in Publication I as well as by using various other existing driving cycles. The energy consumption results were analyzed statistically to acquire novel information about the influence of the various cycle properties on the consumption. Particular focus was put on how the aggressiveness of the driving affects the consumption with the different powertrain options. Additionally, the results provided new insights into which types of powertrains are best suited for different kinds of bus routes. The powertrain topologies compared in the research were diesel, compressed natural gas (CNG), parallel hybrid electric, series hybrid electric, hydrogen fuel cell hybrid electric, and battery electric.

In Publication III, which focuses on BEBs, the energy consumption reductions achieved with different component choices as well as predictive driving were compared. The influence of the driving cycle and ambient temperature on the

effectiveness of the different methods were examined as well. While different factors influencing the energy consumption of electric buses have been examined in previous publications, this type of comparison has not been performed. For the predictive driving, a novel NMPC-based driving optimization that minimizes energy consumption was presented in Publication III. In previous works, the performance of different methods for approximating the efficiency map of the motor and inverter in the NMPC have not been compared. This is another research gap Publication III attempted to fill.

1.4 Outline of the thesis

The remainder of the thesis is structured in the following way. Chapter 2 presents a state-of-the-art review on the research topic. In Chapter 3, the research methods are discussed. The results are presented in Chapter 4, and their implications and reliability are discussed in Chapter 5. Finally, Chapter 6 summarizes and concludes the research.

2. State-of-the-art review

In this chapter, a literature review of previous works on the most relevant research topics is presented. In Section 2.1, previous driving cycle generation methods are discussed, including methods for creating cycles for both passenger cars and city buses. Section 2.2 presents an overview of existing literature on city bus energy consumption and emissions. In Section 2.3, previous publications regarding driving optimization are discussed, including works regarding both passenger cars and city buses.

2.1 Driving cycle generation

Numerous different driving cycles have been created over the years in order to represent the particular route, traffic, and driving style characteristics of various regions. While the cycle generation is always based on measured speed-time data, there are several methods for creating a new cycle based on the data. The driving cycle construction typically includes the following four phases: collecting driving data, segmenting the data, constructing cycles, and finally evaluating and selecting the final cycle [18]. Dai et al. [19] proposed dividing the driving cycle construction methods into four categories: micro-trip-based, segment-based, pattern classification, and modal cycle construction method.

In the first method, the measured data are partitioned into micro-trips. A micro-trip is considered to be the driving between two successive stops. New candidate cycles can then be synthesized by chaining several micro-trips with the aim that the cycle matches the observed data as closely as possible [19]. The synthesis can either be done randomly or based on chosen modal characteristics [20]. Key parameters are chosen for assessing the candidate cycles in order to select the most appropriate candidate as the final cycle. The parameters used in the candidate cycle evaluation can include, for example, average speed, average acceleration, average deceleration, speed-acceleration distribution, power demand distribution, or proportions of low and high-traffic driving [21]–[25]. The values of the key parameters in the candidate cycles are compared to the values found in the entire data set.

The segment-based method differs from the micro-trip-based method in that the driving data are partitioned based on the roadway type and traffic conditions in addition to the stops [26], [27]. Consequently, chaining the segments is more complicated, as the segments can start and end at any speed. Constraints must be set on the speed and acceleration when chaining the segments.

In the pattern classification method, the speed data are divided into kinematic sequences similar to micro-trips [19], [28]. The sequences are then categorized into classes based on specified characteristic parameters. The method considers succession probabilities in considering the likelihood that a segment from one class would precede or follow a segment from a certain other class. Principal component analysis (PCA) and cluster analysis have often been used as part of the pattern classification method [28]–[34]. Two-class Fisher discriminant analysis has also been used instead of PCA and clustering [35]. Multidimensional Markov chains have been proposed to be used for synthesizing cycles [36].

In the modal cycle construction method, driving is viewed as a sequence of acceleration, deceleration, cruise, and idle modes [19], [37]. The measured driving data is partitioned into snippets based on acceleration using a maximum likelihood estimation (MLE) clustering method. The snippets are then classified into modal bins using the MLE clustering method, and the clustering variables include average, minimum, and maximum speeds and accelerations. Then, a transition matrix containing the succession probabilities of the different modes is created, and the cycle is constructed as a Markov chain. When adding a snippet, the next modal bin is selected based on the modal nature of the current snippet and the transition matrix. Additionally, the next snippet is selected from the modal bin such that it optimally improves the speed-acceleration distribution of the new cycle to match that of the entire measured data set.

Although numerous publications have been written about different driving cycle construction methods, the focus has always been on creating a single driving cycle out of a large measurement data set. Methods for creating a large quantity of synthesized cycles for a single route based on limited measurement data have not been developed previously. The research presented here aims to address this research gap by proposing a novel bus driving cycle synthetization method that is capable of generating a large quantity of varying cycles while maintaining the statistical properties found in the original measurement data set.

2.2 City bus energy consumption and emissions

Examining the different factors influencing the energy consumption and emissions of city buses is an important research topic because the viability of different kinds of powertrains can vary significantly based on the region and the types of routes the buses are operated on. Furthermore, understanding the factors that affect the consumption and emissions allows for better optimization of the bus operation, both in terms of designing the bus lines more effectively and driving the bus in a more energy-efficient manner. Reducing costs through more efficient operation is crucial for accelerating the adoption of green city bus technology, as the lifecycle costs are still a significant issue with alternative powertrain options, especially with BEBs and hydrogen fuel cell buses [11], [38].

The energy-production-related factors affecting the emissions of the different city bus powertrain options have been researched extensively. Multiple studies focusing on various parts of the world have demonstrated that the electricity

production methods and local energy availability significantly affect the optimal bus fleet composition [10], [39]–[41]. BEBs can yield the lowest lifecycle emissions of all powertrain options if the electricity production methods are sufficiently clean [10]. However, in the worst-cast scenario with highly polluting electricity production mix, BEBs can cause more lifecycle emissions than diesel buses. On the other hand, hybrid electric buses provide a robust alternative both in terms of energy consumption and emissions regardless of the region they are operated in [39]–[42]. Compressed natural gas can also be a cleaner alternative to diesel, particularly in cases where there are abundant natural gas resources available locally [10]. In order for FCH buses to achieve significant emissions reductions compared to conventional diesel buses, the hydrogen should be produced using electrolysis, and the electricity used for the electrolysis should be generated with greenhouse-gases-free methods [41].

The bus route and ambient conditions have a major impact on the viability of the different powertrain options [13], [14], [43], [44]. Zeng et al. [13] used two different driving cycles in a simulation study where they compared a battery electric, hybrid electric, and diesel bus. The results showed that the energy consumption of the hybrid electric and battery electric buses was less dependent on the driving cycle compared with the diesel bus. In a study comparing data acquired from battery electric and diesel buses operating in Macau, Zhou et al. [14] found similarly that the energy consumption of the battery electric buses increased less during rush hours compared with the diesel buses. Stop maneuvers are highly energy-consuming with internal combustion engine (ICE) vehicles due to the inability to perform regenerative braking. Nonetheless, the stop frequency is still one of the most influential factors affecting the energy consumption of BEBs [45]. Furthermore, it has been shown that BEBs tend to be driven more aggressively than diesel buses due to the power delivery characteristics of electric motors (EMs) [46]. Additionally, increases in the passenger load magnify the effect of the aggressiveness on the energy consumption [47]. On the other hand, the consumption of hybrid electric and battery electric buses is proportionally more affected by the air conditioning (AC) system [16], [48]. Heating the cabin is a particularly important issue with BEBs, as there is significantly less waste heat available from the electric powertrain compared to a diesel engine, requiring part of the battery energy to be sacrificed for heating when the ambient temperature is low [16], [49]–[52]. A fuel heater may be used instead, but it is a poor compromise due to the resulting pollution. The heating and cooling of the battery pack also increases the sensitivity of hybrid electric buses and especially BEBs to ambient temperature fluctuations. Consequently, the power demand fluctuations caused by variations in the ambient temperature should be carefully considered when evaluating the viability of BEBs [53].

Heat pumps have been suggested as a potential key technology for improving the thermal efficiency of the heating, ventilation, and air conditioning (HVAC) systems in BEBs in the coming years as the technology matures [16]. Reducing the energy consumption is particularly important with BEBs due to the size and mass of the battery pack being bound to the energy capacity requirement. Other

potential ways to reduce the consumption include reducing the rolling resistance with better tires and reducing the aerodynamic drag with a lower body shape. A simulation study conducted by Lajunen and Tammi [47] showed rolling resistance to cause 25-30 % and aerodynamic drag 3-25 % of the total energy losses of a BEB during driving.

Currently, hybrid electric buses are generally a more competitive alternative than BEBs to conventional diesel buses in terms of lifecycle costs [11], [38]. However, BEBs are gradually closing the gap, and in ideal operating conditions they can already be more cost-effective than diesel buses [11], [54]. It is expected that BEBs will become more cost-effective than both diesel and hybrid electric buses under most conditions in the 2020s. Lifecycle costs are still the most significant issue for FCH buses, as the total cost of ownership of an FCH bus is approximately twice as high as that of a diesel bus [11], [38]. FCH buses are projected to gradually become more cost-effective, but the lifecycle costs are not expected to have decreased to the same level with diesel buses even by 2030 [11].

While the various city bus powertrain options have been compared from a multitude of perspectives in previous works, there has not been any significant focus on the influence of driving cycle uncertainty and passenger load variations on the energy consumption. The consumption fluctuations on a single bus route caused by driving cycle and passenger load uncertainty have not been analyzed in-depth. Previous simulation studies have only used a limited number of generic driving cycles. The research gap is addressed in the work presented here by using the novel cycle synthesis method to produce a large quantity of varying cycles and passenger loads for a typical suburban Finnish bus route and simulating them with validated bus models that feature the most common alternative powertrain topologies. Additionally, the effect of the different driving cycle parameters on the energy consumption of alternative powertrains is exhaustively examined in this research. In order to study the effect of the different cycle properties, variance decomposition is used. Particular focus is put on how the aggressiveness of the driving affects the consumption with the various powertrain types. The aggressiveness is given a mathematical definition in order to quantify it.

Another research gap this study aims to address is the lack of a direct comparison of the effectiveness of the different component-choice-related methods for reducing the energy consumption of city buses. In this research, the consumption reductions achieved with a lightweight aluminum chassis, low-rolling-resistance tires, low-drag body, and heat pump are compared using a simulation model of a BEB. The influence of ambient temperature on the effectiveness of the different methods is also considered. Furthermore, the consumption reductions achievable with predictive driving are compared to the energy savings of the aforementioned methods.

2.3 Driving optimization

Dynamic programming (DP) has been used for non-real-time driving optimization in various publications. The works have mostly centered on passenger cars [55]–[57]. Lajunen [58] created a distance-based DP driving optimization algorithm for optimizing existing cycles for electric and diesel buses to minimize energy consumption. The simulation study showed that on the well-known Braunschweig (BR) test cycle the driving profile optimization could increase the energy efficiency of a BEB by 17 % and diesel bus by 19 %. Because DP is highly computationally-intensive, it has been generally considered unsuited for real-time optimization [59]. However, using cloud computing to enable real-time optimization with DP algorithms has been proposed [60]. Additionally, Doan et al. [61] developed an iterative DP algorithm with an adaptive objective function for electric vehicles (EVs) that they showed to be fast enough for real-time operation. Additionally, quadratic programming (QP) has been proposed to be used in driving optimization with the use of two-stage optimization [59]. In the first stage, the driving profile of the full route would be defined before the start of the trip. Then, short-term optimization would be performed on route in real-time in order to account for the current traffic conditions.

Model predictive control (MPC) has been utilized for several different vehicular applications, including yaw control, path planning, tracking and collision avoidance, traffic management, thermal management, charging optimization, transmission control, as well as hybrid electric vehicle power management [62]–[72]. MPC has also been employed for real-time driving optimization with various types of powertrains. Using NMPC with a third-degree polynomial approximation of the fuel consumption as a function of speed and acceleration has been proposed for ICE vehicles [73]. A similar approach was taken in a study where an NMPC driving optimization algorithm was developed for a plug-in power split hybrid electric vehicle. The algorithm approximated the fuel consumption as a function of engine output power and vehicle speed with a second-degree polynomial. In order to limit the computational load of the algorithm, the efficiencies of the EMs were approximated as constant. Linear and explicit MPC algorithms have been developed for EVs [74], [75]. Utilizing a Bayes network model to predict the movement of the preceding vehicle in MPC driving optimization applications has also been proposed [75].

Only limited research has been conducted in the field of MPC driving optimization of electric vehicles, and NMPC has not been employed for EVs. The work presented here aims to fill that research gap by presenting a novel driving optimization problem formulation for NMPC. Furthermore, the performance of different methods for approximating the efficiency map of the EM and inverter are compared in this study.

3. Methods

3.1 Overview

The main research method in this thesis is simulation studies. In Publication I, a simulation model of a BEB was developed for Simulink using a detailed space-vector model for the electric motor and inverter. The simulated bus was parametrized to match an electric bus operating on the Espoo 11 bus line in Finland. Data were acquired from the electric bus via an Internet of things (IoT) system. The output voltage, current, and state-of-charge (SOC) of the battery of the real bus were compared to those of the simulated model on the same driving cycle in order to validate the model. Other driving cycles were recorded for the purpose of using them in a novel driving cycle synthesis algorithm. The stochastic cycle synthesis is capable of creating a large quantity of varying driving cycles for the same bus route, allowing for the acquisition of a realistic energy consumption distribution for the route. The simulation model was used to run 10000 synthetic cycles in order to acquire an energy consumption distribution for the route. The correlations between the energy consumption and various cycle parameters were then analyzed using the Pearson correlation coefficient. Furthermore, Global Sensitivity Analysis (GSA) was used to examine the influence of the stop frequency and passenger load on the energy consumption.

In Publication II, the Autonomie vehicle simulation software (revision 14) was used. Autonomie is a MATLAB-based software environment and framework for automotive control-system design, simulation, and analysis [76]. The revision of the software used in this research was running on version R2012 of MATLAB. Predefined powertrain architectures and libraries for powertrain components are provided in the Autonomie software. Furthermore, component initialization data are supplied, including for heavy vehicles. Six city bus models were created: diesel, CNG, parallel hybrid electric, series hybrid electric, FCH, and battery electric. The models were based on those used by Lajunen and Lipman [11]. However, the powertrains of the diesel, series hybrid, FCH, and battery electric buses were reconfigured, and the masses of the buses were changed. The masses were chosen based on the specifications of real buses such that the differences in the masses between the different models would be realistic [77]–[81]. The hybrid models were of the non-plug-in type. The electric powertrain was validated using data acquired from an electric bus operating in Helsinki. Additionally, the same electric motor and inverter were used in the series hybrid and FCH models. Furthermore, dynamometer data were supplied by VTT Technical Research Centre of Finland for a diesel bus. The data were used to validate the

powertrain of the diesel bus model. Three thousand synthetic cycles for the Espoo 11 bus line were generated using the cycle synthesis algorithm developed in Publication I. The synthetic cycles were then run with each bus model. Furthermore, a collection of 20 existing cycles used in previous studies were utilized to conduct a separate analysis. The results were analyzed statistically in order to examine the influence of the various driving cycle properties and passenger load on the energy consumption with the different bus types. The statistical analysis was conducted using Pearson correlation coefficients and multiple linear regression (MLR) based variance decomposition. Additionally, a mathematical definition was given for the aggressiveness of the driving in order to observe the effect of the driving style on the energy consumption.

Publication III focuses only on electric buses. A new BEB simulation model was developed in Simulink. The main difference between the models employed in Publication I and III is that in the latter case an efficiency-map-based model was used for the electric motor and inverter rather than the more complex space-vector model used in Publication I. Furthermore, the battery model was simplified in Publication III. The aim of these changes was to make the model significantly computationally lighter. Four key component-choice-related methods for reducing the energy consumption were chosen, and they will be described in Section 3.6. The methods were tested one at a time by changing the related parameter values. The changes in the values of the parameters were estimated based on previous works [15]–[17], [47], [78], [82]–[84]. Furthermore, in order to examine the energy consumption reductions achievable with predictive driving, a driving optimization algorithm was developed in MATLAB and Simulink using the Model Predictive Control Toolbox. Fifteen different driving cycles and two ambient temperature settings were used in the simulation tests in order to investigate the influence of driving cycle and ambient temperature on the effectiveness of the energy consumption reduction methods.

The methods used are described in this chapter. First, the methods used for acquiring driving cycles and validation data for the simulated city bus models are discussed in Section 3.2. The simulation models are then described in detail in Section 3.3. Section 3.4 presents the existing driving cycles used in Publications II and III as well as the driving cycle synthesis algorithm developed in Publication I and also utilized in Publication II. In Section 3.5, the statistical analysis methods used in the publications are described. In Section 3.6, the component-choice-related methods for reducing the energy consumption of city buses tested in Publication III are discussed. Finally, Section 3.7 presents the NMPC driving optimization algorithm developed in Publication III.

3.2 Data acquisition

Data were collected from a BEB operating on bus line 11 in Espoo, Finland, the route of which is shown in Figure 2, for the purposes of the driving cycle synthetization in Publications I and II and powertrain validation in Publication I. The bus line operated up until early 2018 between Friisilä and Tapiola. The elec-

tric buses operating on the line were recharged at a fast-charging station at Tapiola. The research in this thesis focuses on the direction from Friisilä to Tapiola. The Espoo 11 (E11) route can be considered a typical Finnish suburban bus route because it travels between smaller suburban centers and also features short urban sections as well as roads with slightly higher speed limits. The bus line featured 25 bus stops.

The signals collected included the battery current, voltage, and SOC estimate, as well as the speed of the bus, the auxiliary device power consumption, and the Global Positioning System (GPS) coordinates. The speed was acquired from the anti-lock brake system controller unit. The sampling rates of the different measurements can be seen in Table 1. The battery current, voltage, SOC, and auxiliary power were only acquired for one cycle for the purpose of validating the simulation model. The other signals were recorded for 23 additional driving cycles in order to have a collection of cycles that the cycle synthesis could be based on. The recorded driving cycles occurred between 27 December 2016 and 6 February 2017. The mean temperature during the measured cycles was 0.3 °C. The temperature ranged from -10 to 4.8 °C. The driving cycles were obtained only from weekdays because the bus did not run on weekends. Additionally, passenger numbers were logged on 37 runs of the route. The runs took place between March 2016 and February 2017. The passengers were logged manually by travelling in the bus, as there was no system available for automatically logging the passengers with the IoT system.

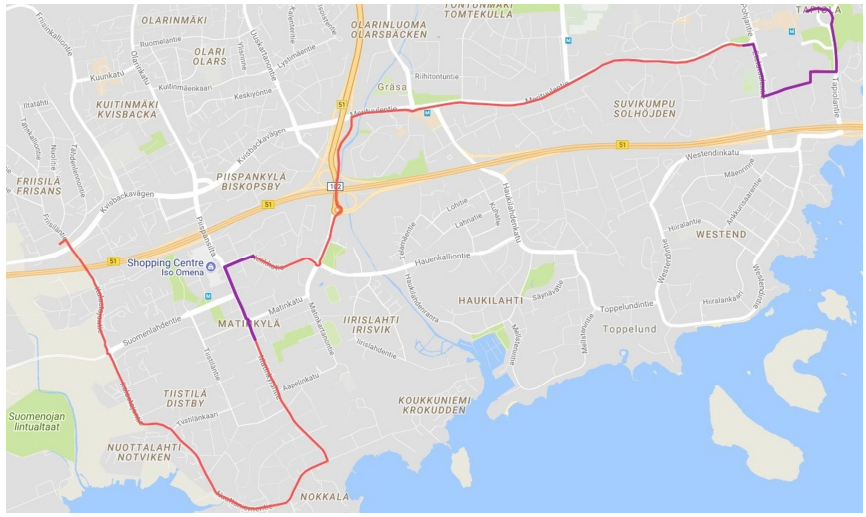

Figure 2. Bus line 11 in Espoo, Finland. Purple sections indicate urban areas. (Map data ©2018 Google) (Publication II).

Table 1. IoT data collection system signal sampling rates (Publication I).

Sampling rate	Signal
2 Hz	Battery current
1 Hz	Speed, battery voltage
0.2 Hz	GPS coordinates, SOC estimate, auxiliary device power demand

Figure 3 presents an example of an E11 cycle as well as the well-known Braunschweig (BR) bus test cycle for comparison. The purple portions in the E11 cycle indicate the urban sections. The altitude profile of the E11 route is also presented in the figure. The roads featured on the route are generally either flat or gently sloping; the steepest uphill is only 4.0 degrees and the steepest downhill -3.6 degrees. The characteristic parameters of the E11 route are compared to those of the BR cycle in Table 2. The BR cycle was deemed to be a good comparison point despite representing urban driving, as it features comparable characteristics and it has been widely used in existing literature, for example in references [11], [42], [83], and [84]. The E11 parameters in Table 2 are the average values calculated based on all of the 24 measured cycles.

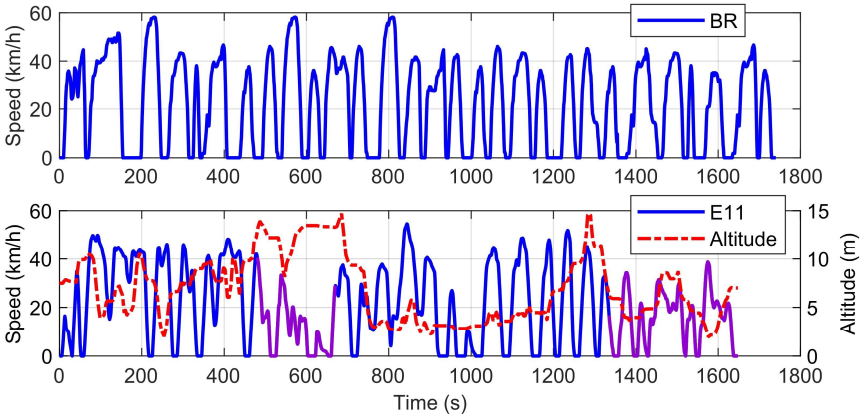

Figure 3. BR cycle and an example of a measured E11 cycle. Purple sections in the E11 cycle indicate urban areas (Publication II).

Table 2. BR and E11 characteristic parameters (Publication II).

Parameter	BR	E11
Max. speed (km/h)	58.2	54.8
Average speed (km/h)	22.5	21.8
Average driving speed (km/h)	29.5	26.2
Distance (km)	10.9	9.74
Stops per km	2.6	2.1
Duration (s)	1740	1637
Total stop time (s)	412	283
Avg. stop duration (s)	14.2	12.9
Creep percentage	1.7 %	1.8 %
Cruise percentage	12.8 %	15.2 %
Idle percentage	23.7 %	16.8 %
Max. acceleration (m/s^2)	2.41	1.44
Max. deceleration (m/s^2)	3.58	1.81
Avg. acceleration (m/s^2)	0.54	0.46
Avg. deceleration (m/s^2)	0.72	0.43
Aggressiveness (m/s^2)	0.22	0.19

The aggressiveness of the driving cycle was calculated as [87]:

$$A = \sum_{i=1}^{n} \int_{t_{i,1}}^{t_{i,2}} (a \cdot v)\, dt / d_c, \tag{1}$$

where a is the positive forward acceleration, v is the speed, n is the number of periods of positive acceleration, $t_{i,1}$ is the start of the i-th positive acceleration period and $t_{i,2}$ is the end of said period, and d_c is the total distance of the driving cycle. This definition was considered to be logical, as it emphasizes excessive accelerations performed at high speeds. Creep and cruise, found in Table 2, were defined as:

Creep: $0 < v \leq 4$ km/h & $|a| \leq 0.1$ m/s^2
Cruise: $v > 4$ km/h & $|a| \leq 0.1$ m/s^2

Additionally, measurement data were acquired via the IoT system from the same electric bus model operating on bus line 55 in Helsinki for validating the electric powertrain in Publication II. Data from one driving cycle of the route were gathered, and the sampling rate was 0.2 Hz. The cycle included the full route from Koskela to the Helsinki Railway Square and back to Koskela. The ambient temperature during the measured cycle was 22.4 °C. The number of passengers in the bus during the validation cycle was obtained from HSL.

Furthermore, measurement data were acquired for a diesel bus from dynamometer tests conducted by VTT Technical Research Centre of Finland. The VTT laboratory features a calibrated chassis dynamometer, and the measurement procedures have been accredited. The BR driving cycle was simulated using the dynamometer with the sampling rate of the measurements being 10 Hz. The speed and fuel rate were logged for validating the diesel powertrain in Publication II. The average ambient temperature during the measurements was 23.0 °C.

3.3 City bus simulation models

In this section, the modeling of the city buses is discussed. The focus is mostly on the models used in Publications I and III, as the models were built from scratch. In Publication II, the Autonomie models utilized were based on those used in reference [11], but they were reparametrized for the purposes of the research.

The longitudinal dynamics are discussed first in Section 3.3.1. The same longitudinal dynamics model was employed in the models used in Publications I and III. The simple efficiency-map-based electric motor and inverter model used in Publication III is discussed in the same section. The more detailed space-vector model used in Publication I is then discussed in Section 3.3.2. The battery models are described in Section 3.3.3. Finally, simulation model parameters and model validation are discussed in Sections 3.3.4 and 3.3.5.

3.3.1 Longitudinal dynamics and powertrain models

The city buses were modeled in the time domain. It was assumed that the buses only travel forward; reversing was not considered in the models. The acceleration of the vehicle is calculated as:

$$a = \frac{dv}{dt} = \frac{F_w - F_R}{m + J_t/r_d^2} \tag{2}$$

where, v is the speed of the vehicle, t is time, F_w is the tractive force at the driven axle, F_R is the total resistive force, m is the total mass of the vehicle, J_t is the total moment of inertia superimposed at the driven axle, and r_d is the dynamic radius of the wheels. The total resistive force is calculated as the sum of the rolling resistance (F_{rr}), gravitational force (F_G), and aerodynamic drag (F_d):

$$F_R = F_{rr} + F_G + F_d. \tag{3}$$

The rolling resistance is defined as:

$$F_{rr} = mgf_{rr}\cos(\alpha)\,\mathrm{sign}(v) \tag{4}$$

where g is the gravitational acceleration, which was defined as 9.81 m/s² in this research, f_{rr} is the rolling resistance coefficient, and α is the road grade. The gravitational force resisting the longitudinal motion of the vehicle is:

$$F_G = mg\sin(\alpha). \tag{5}$$

The aerodynamic drag is calculated as:

$$F_d = \frac{1}{2}\rho c_D A v^2 \tag{6}$$

where ρ is the density of air, c_D is the aerodynamic drag coefficient, and A is the frontal area of the vehicle. The tractive force at the driven axle is defined as:

$$F_w = T_{EM} i_g i_{fd} H_{dt}/r_d + F_B \tag{7}$$

where i_g is the gear ratio of the gearbox, i_{fd} is the gear ratio of the final drive, F_B is the mechanical braking force, and T_{EM} is the output torque of the electric motor. The variable H_{dt} in equation (7) represents the efficiency of the drivetrain, and it is defined in the following way:

$$\begin{cases} H_{dt} = \eta_g \eta_{fd}, & P_{EM,out} \geq 0 \\ H_{dt} = 1/(\eta_g \eta_{fd}), & P_{EM,out} < 0 \end{cases} \tag{8}$$

where η_g is the efficiency of the gearbox, η_{fd} is the efficiency of the final drive, and $P_{EM,out}$ is the power output of the EM, which is calculated as:

$$P_{EM,out} = T_{EM}\omega_{EM} \tag{9}$$

where ω_{EM} is the rotational speed of the output shaft of the electric motor. The rotational speed can be calculated as:

$$\omega_{EM} = v i_g i_{fd} / r_d. \tag{10}$$

The space-vector model used for the electric motor and inverter in Publication I is discussed in Section 3.3.2. In Publication III, an efficiency-map model was used instead for the EM of the simulated bus model. The map also included the efficiency of the inverter. In the EM efficiency map, the efficiency is represented as a function of the output torque and rotational speed. The electrical input power of the EM is defined according to the following equation:

$$\begin{cases} P_{EM,in} = P_{EM,out} / \eta_{EM}, & P_{EM,out} \geq 0 \\ P_{EM,in} = P_{EM,out} \eta_{EM}, & P_{EM,out} < 0 \end{cases} \tag{11}$$

where η_{EM} is the efficiency of the electric motor and inverter at the current operating point. The efficiency map is shown later in Section 3.7 in Figure 12. The EM output torque was configured such that it would respond to the torque demand with a minor delay by using the following transfer function:

$$T_{EM} / T_{EM,req} = 1/(\tau s + 1) \tag{12}$$

where τ is the time response of the motor, s is the Laplace-domain variable, and $T_{EM,req}$ is the torque requested by the motor controller. The time response was configured as 0.05 s. The torque request would come from a proportional controller in the case of the component-choice-related simulations. Excess negative torque requested would be converted to mechanical braking force. In the NMPC simulations, the torque and mechanical braking force requests would be provided by the nonlinear model predictive controller.

3.3.2 Electric powertrain space-vector model

The battery electric bus model developed for Publication I employs a space-vector model for the EM and inverter. The topology of the model is presented in Figure 4. In the model, the sinusoidal phase voltages and currents are fixed to the rotor coordinates using the direct-quadrature (dq) transformation. The electric motor model omits hysteresis losses and eddy currents.

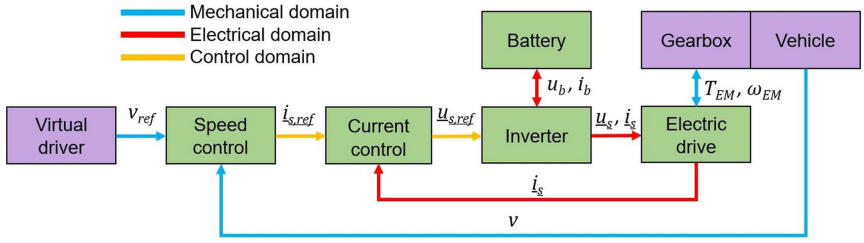

Figure 4. Topology of the BEB simulation model employed in Publication I (adapted from [88]).

The operation of the permanent magnet synchronous machine (PMSM) is principally governed by the following equations [88]:

$$\underline{u}_s = R_s \underline{i}_s + d\underline{\psi}_s/dt + \mathrm{j}\omega_m \underline{\psi}_s \tag{13}$$

$$\underline{\psi}_s = L_s \underline{i}_s + \psi_f \tag{14}$$

$$T_{EM} = 3p/2 \cdot \mathrm{Im}\left\{\underline{i}_s \underline{\psi}_s^*\right\} = 3p\psi_f i_q/2 \tag{15}$$

$$\omega_m = \omega_{EM} p \tag{16}$$

where $\underline{u}_s$ and $\underline{i}_s$ are the stator voltage and current, $\underline{\psi}_s$ is the stator flux linkage, ω_m is the electrical angular speed of the rotor, ψ_f is the permanent flux induced by the magnets, i_q is the q-axis current, R_s is the stator resistance, L_s is the stator inductance, and p is the number of pole pairs. The current is limited according to the following equation [89]:

$$i_s^2 = i_d^2 + i_q^2 \leq i_{max}^2 \tag{17}$$

where i_d is the d-axis current and i_{max} is the maximum allowed stator current. In steady-state, the stator voltage can be approximated as [89]:

$$\underline{u}_s = \mathrm{j}\omega_m \underline{\psi}_s = \mathrm{j}\omega_m\left(L_s \underline{i}_s + \psi_f\right) = \mathrm{j}\omega_m\left(L_s i_d + \psi_f + \mathrm{j}L_s i_q\right) \tag{18}$$

by assuming $R_s = 0$. Thus, the voltage limit can then be expressed as [89]:

$$u_s^2 = \omega_m^2 \psi_s^2 \leq u_{max}^2 \tag{19}$$

where u_{max} is the maximum allowed stator voltage. By combining equations (18) and (19), a limit for the stator flux linkage can be solved as [89]:

$$\psi_s^2 = \left(L_s i_d + \psi_f\right)^2 + \left(L_s i_q\right)^2 \leq \frac{u_{max}^2}{\omega_m^2}. \tag{20}$$

It can be seen in equation (20) that higher speeds can be reached by setting $i_d < 0$. This is known as field weakening [89]. Below the speed at which field weakening needs to be activated, the d-axis current is set to zero by the current controller. The total current is always limited by equation (17). Hence, the available maximum torque is reduced in the field-weakening operating region, as the maximum q-axis current is limited and the torque is dependent on the q-axis current, as is shown in equation (15). The input power of the motor is calculated as [89]:

$$P_s = \frac{3}{2}\mathrm{Re}\{\underline{u}_s \underline{i}_s^*\}. \tag{21}$$

The PI speed controller in Figure 4 outputs the torque request, which is then converted into stator current by solving the q-axis current from equation (15):

$$i_q = \frac{2T_{EM,req}}{3p\psi_f}. \tag{22}$$

The torque request is limited by the torque and mechanical output power limits imposed on the EM. Any excess negative torque requested is converted to mechanical braking force.

3.3.3 Battery models

Two different models were used for the batteries; resistor model and Thévenin model. The Thévenin model was used in Publication I and the resistor model in Publication III. The Thévenin model is depicted in Figure 5.

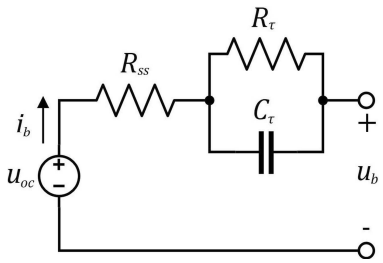

Figure 5. Thévenin circuit model for a battery.

In the Thévenin model, the total internal resistance of the battery consists of two components; the steady-state resistance component (R_{ss}) and the transient component (R_τ). The operation of the battery is governed by the following equations:

$$u_b = u_{oc} - R_{ss} i_b - u_{C_\tau} \tag{23}$$

$$\frac{du_{C_\tau}}{dt} = \frac{1}{C_\tau}\left(i_b - u_{R_\tau}/R_\tau\right) \tag{24}$$

$$u_{R_\tau} = u_{C_\tau} \tag{25}$$

$$i_b = \begin{cases} P_{aux}/u_b + P_s/(u_b \eta_i), & P_s \geq 0 \\ P_{aux}/u_b + P_s \eta_i/u_b, & P_s < 0 \end{cases} \tag{26}$$

where u_b is the output voltage of the battery, u_{oc} is the open-circuit voltage, u_{C_τ} is the voltage over the capacitor, C_τ is the capacitance of the capacitor, u_{R_τ} is the voltage over the transient resistance component, P_{aux} is the auxiliary device power demand, and η_i is the inverter efficiency, which was configured to be dependent on the torque and speed of the EM. The efficiency map used for the inverter can be found in reference [88]. The open-circuit voltage is dependent on the SOC of the battery. The SOC of the battery (q_b) is calculated as:

$$\frac{dq_b}{dt} = \frac{i_b}{3600 C_b} \tag{27}$$

where C_b is the total energy capacity of the battery in ampere hours.

The resistor model is a simplified version of the Thévenin model, as it omits the transient behavior of the battery. Based on the model created for Publication

I, it was determined that the transient effects have minimal influence on the energy consumption, and therefore it was deemed appropriate to simplify the model to make it computationally lighter. The resistor model, which is depicted in Figure 6, is described by the following equations:

$$i_b = \frac{u_{oc} - \sqrt{u_{oc}^2 - 4R_{int}\left(P_{EM,in} + P_{aux}\right)}}{2R_{int}} \tag{28}$$

$$u_b = u_{oc} - R_{int} i_b \tag{29}$$

where R_{int} is the internal resistance of the battery. The SOC is calculated using equation (27). The resistor model takes the battery output power as its input and calculates the current, voltage, and SOC.

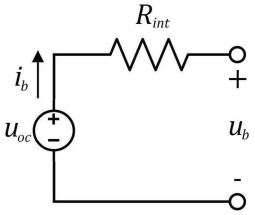

Figure 6. Resistor model for a battery.

In both battery models, the energy consumption is calculated as:

$$E = \int u_{oc} i_b \, dt. \tag{30}$$

3.3.4 Simulation model parameters

In Publication I, the simulation model of a battery electric bus developed in Simulink was parametrized according to the vehicle the data was acquired from. The parameter values are presented in Table 3. The power demand caused by the auxiliary devices was configured to be equal to the average demand measured in the validation cycle. The auxiliary power demand does not include the separate diesel heater, as measurement data was not available from the heater. The ambient temperature was defined as -6 °C for the simulations, which was the average ambient temperature during the validation cycle. The mass of a passenger was set to 70 kg.

In Publication II, the Autonomie simulation software was employed. The city bus simulation models were based on the models used by Lajunen and Lipman in reference [11]. The battery electric powertrain was reconfigured to match that of the bus the validation data had been acquired from. The electric powertrain, excluding the battery pack, was implemented in the FCH and series hybrid models as well. The diesel bus powertrain was reparametrized to match that of the bus that had been used in the dynamometer measurements discussed in Section

3.2. The validation procedures of the electric and diesel powertrains are presented in Section 3.3.5. The parameter values of the six bus models are shown in Table 4 and Table 5. The masses of the models were configured based on real bus specifications such that the differences in the masses would be realistic. The mass of the BEB, which was chosen to equal the mass of the electric bus that the validation data were acquired from, was selected as the baseline. The masses of the diesel, parallel hybrid electric, and battery electric powertrains were estimated to be approximately equal based on references [77]–[79]. The BEB is of the opportunity-charging type, meaning that the size of the battery pack is relatively small. An overnight-charging type bus would be significantly heavier due to the larger battery pack. The fuel cell hybrid electric powertrain was estimated to be 1630 kg heavier than the diesel powertrain based on specifications found in reference [81]. The masses of the CNG and series hybrid electric buses relative to the diesel bus were estimated based on reference [80]. In the synthetic E11 cycles, the mass of a passenger was set to 68 kg based on Federal Transit Administration (FTA) bus testing regulations [90]. On the 20 existing bus cycles that are presented in Section 3.4.2, a payload of 440 kg was used, as that was the average passenger load in the synthetic cycles. The chassis dimensions as well as the drag and rolling resistance coefficients were defined identically for the six models. The parameters were left at the same values used by Lajunen and Lipman in reference [11]. The ambient temperature was set to 22.5 °C.

Table 3. Parameters of the BEB simulation model used for the initial driving cycle uncertainty simulations in Publication I.

Category	Parameter	Value
General	Curb weight (kg)	10500
	Vehicle frontal area (m^2)	6.2
	Coefficient of drag	0.5
	Differential gear ratio	4.93
	Differential gear efficiency (%)	98
	Tire dynamic radius (m)	0.43
	Total inertia at motor output axle (kgm^2)	1.95
	Rolling resistance coefficient	0.008
	Air density (at -6 °C) (kg/m^3)	1.32
	Total average auxiliary power demand (excluding diesel-powered heater) (kW)	5.16
Battery pack	Nominal voltage (V)	690
	Capacity (kWh)	55.2
	Internal resistance (mΩ)	87.5
	Internal capacitance (F)	0.56
Electric motor	Number of pole pairs	6
	Flux induced by the permanent magnets (Vs)	0.4
	Stator armature inductance (mH)	0.3
	Stator resistance (mΩ)	157
	Maximum motor power (kW)	180

Table 4. Common parameters of the models used in Publication II.

Parameter	Value
Vehicle frontal area (m^2)	7.24
Drag coefficient	0.79
Rolling resistance 1st coefficient	0.008
Rolling resistance 2nd coefficient (1/(m/s))	0.00012

Table 5. Parameters of the simulation models used in Publication II.

Parameter	Diesel	CNG	Par. hybrid	Ser. hybrid	Electric	FCH
Curb weight (kg)	10500	11630	10500	11630	10500	12130
ICE peak power (kW)	235	205	160	160	-	-
EM peak power (kW)	-	-	167	180 / 270 (regen.)	180 / 270 (regen.)	180 / 270 (regen.)
Fuel cell power (kW)	-	-	-	-	-	160
Battery capacity (kWh)	-	-	7.7	11.6	55.2	11.6
Battery nom. voltage (V)	-	-	648	648	690	648
Batt. cell config. (series x parallel)	-	-	180 x 2	180 x 3	300 x 4	180 x 3
Transmission	6-speed automatic	6-speed automatic	12-speed automatic	Fixed gear ratio	Fixed gear ratio	Fixed gear ratio
Aux. power (kW)	4 (mech.) 1 (elec.)	4 (mech.) 1 (elec.)	1 (mech.) 4 (elec.)	1 (mech.) 4 (elec.)	4 (elec.)	4 (elec.)

The parameter values of the simulation model used in Publication III were selected to represent a generic electric bus. The values, which are shown in Table 6, were chosen based on reference [47]. The aerodynamic drag value given in the table is the product of the frontal area and drag coefficient. Two ambient temperature settings were used in Publication III: -10 and 20 °C. The HVAC power demand at each temperature was defined based on a graph found in reference [47].

Table 6. Specifications of the BEB simulation model used for the energy consumption reduction and NMPC simulations in Publication III.

Parameter	Value
Bus curb weight (kg)	12350
Passenger load (kg)	415
Aerodynamic drag (m^2)	6.12
Rolling resistance coefficient	0.008
Battery energy capacity (kWh)	77.3
Motor nominal power (kW)	170
Motor max peak torque (Nm)	1710
Constant aux. power without HVAC (kW)	5.0
HVAC power at -10 °C (kW)	7.0
HVAC power at 20 °C (kW)	2.0
Gear reduction	1.75
Final drive ratio	4.72
Tires	275/70/22.5
Tire dynamic radius	0.478

The acceleration and speed limits for regenerative braking were defined identically for all the models capable of regenerative braking used in the three publications. The limits can be seen in Table 7. Full regeneration is chosen when the conditions for both modes are met. In the partial regeneration mode, the maximum regeneration power is limited. When the speed falls below 10.8 km/h, the limit is reduced linearly with speed until no regeneration is allowed below 5.4 km/h. The deceleration limit works in the same fashion in that the maximum regeneration power is reduced linearly with deceleration beyond 2.5 m/s^2 until no regeneration is permitted above a deceleration of 4.0 m/s^2.

Table 7. Regenerative braking limits of the battery electric and hybrid electric models used in all of the simulations.

	Partial regeneration	Full regeneration
Speed (m/s)	$v \geq 1.5$	$v \geq 3.0$
Acceleration (m/s^2)	$0 > a \geq -4$	$0 > a \geq -2.5$

3.3.5 Simulation model validation

In Publication I, the model was validated by using data from one run of the Espoo 11 bus route. The battery SOC, voltage, and current were compared between the measurement data and the simulation model (Figure 7). The SOC reduced by 19.77 % during the simulated cycle compared to a 19.80-% reduction in the measured cycle. The voltage in the simulation model had a root-mean-square error (RMSE) of 3.50 V. The RMSE of the simulated current was 21.89 A.

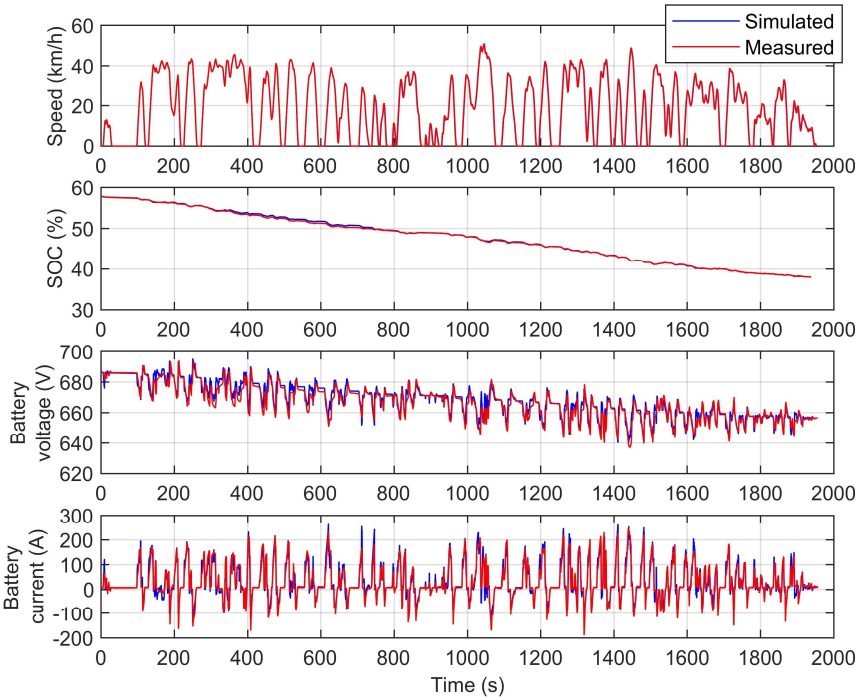

Figure 7. Validation of the BEB simulation model used for the initial driving cycle uncertainty simulations (Publication I).

In Publication II, the simulation model of a diesel bus was validated by comparing the measured fuel rate and total fuel consumption to the simulated fuel rate and consumption on the Braunschweig cycle (Figure 8). The total mass of the bus used in the dynamometer measurements was 19500 kg, which included a 4750 kg payload. The total mass of the simulation model was set to the same value for the validation. The RMSE of the fuel rate of the simulation model was 5.06 l/h. The energy consumption was computed based on the fuel rate by assuming the density of diesel as 0.84 kg/l and the heating value as 42.5 MJ/kg. The values are the default values used by the Autonomie software. The energy consumption during the simulated cycle was 61.26 kWh, while the measured consumption was 61.44 kWh. Hence, the error of the simulated consumption was 0.3 %.

The BEB simulation model was validated with the data acquired from an electric bus operating on the Helsinki 55 bus line. The validation was performed by comparing the SOC during the simulated and measured cycles (Figure 9). The

SOC reduced by 23.04 % during the measured cycle and by 23.02 % in the simulated cycle. The RMSE of the SOC of the simulation model was 0.52 %. The validated electric powertrain, excluding the battery pack, was also used in the FCH and series hybrid models. The deviation of the simulated SOC from the measured SOC in the middle part of the cycle was assumed to have been caused by inaccuracy in the altitude profile because the cycle included the entire back-and-forth route.

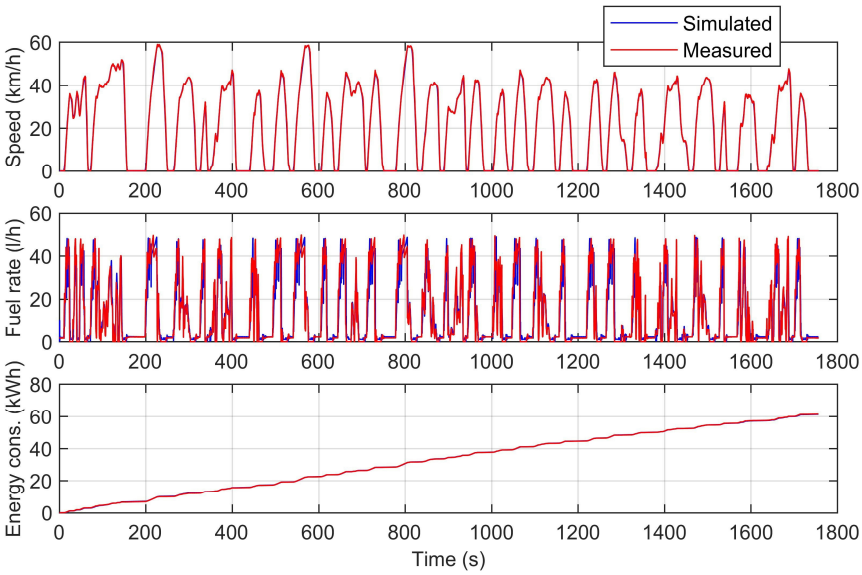

Figure 8. Validation of the diesel bus (Publication II).

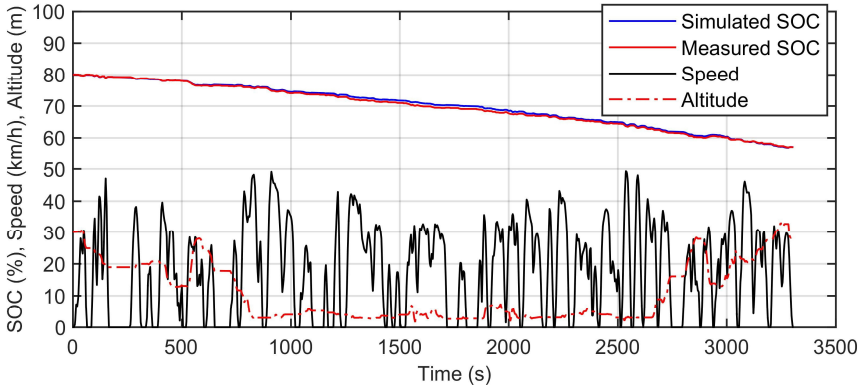

Figure 9. Battery electric bus simulation model validation (Publication II).

3.4 Driving cycles

In this section, the driving cycle algorithm used in Publications I and II as well as the other existing cycles utilized in Publications II and III are discussed.

3.4.1 Driving cycle and passenger load synthetization

A driving cycle synthetization algorithm was developed for the purpose of being able to obtain a large quantity of varying cycles for a single bus route based on only a handful of measured cycles. The original concept of the segment-based driving cycle synthetization method was developed by Joel Anttila and presented in [91]. The synthetization algorithm developed in the research presented here is an expansion of the previous concept created by Anttila. The goal of the synthetization process is to produce synthetic cycles that maintain the statistical properties of the original measured cycles as accurately as possible.

In the synthetization, the measured cycles are first divided into segments that begin and end at subsequent bus stops regardless of whether the bus stopped at the stop or not. New cycles are then constructed by chaining together segments from the measured cycles. Only the respective segments can be used, meaning that only the *i*-th segment in the measured cycles can be selected for the *i*-th segment in the new synthetic cycle. Hence, the number of segments is the same in every cycle. The bus stops the vehicle will stop at during the new synthetic cycle are randomized. The likelihood of stopping at each bus stop is determined based on the probabilities found in the measurements. When the segments are chained together, various scenarios can occur based on whether the bus stopped at the bus stop in the measured cycles and whether or not a stop is performed there in the new synthetic cycle.

If a synthetic deceleration or acceleration maneuver needs to be created in order to create a stop maneuver, the acceleration is sampled from a distribution based on the measured cycles. When an artificial driving maneuver is created in order to skip a stop, the acceleration in the artificial portion is limited to a maximum absolute value of 1.1 m/s². The limit was selected based on previous publications on the topic of passenger safety and comfort [92], [93]. It was assumed bus drivers tend to avoid exceeding the 1.1 m/s² limit. Additionally, the segments are chained together in such a way that there is minimal variation in the total distance of the cycle. The flow chart of the synthetization process is shown in Figure 10, which includes both the data analysis and synthetization phases. The analysis phase must be finished before the synthesis can begin. The full description of how the segment-chaining is performed can be found in Publication I. In Publication I, 10000 synthetic E11 driving cycles were used, and 3000 E11 cycles were synthesized in Publication II. The 24 cycles measured from the E11 route discussed in Section 3.2 were used as the basis of the synthetization.

The number of passengers in the bus is also randomized. The randomization is performed in two phases in such a way that the correlation between the number of stops and average passenger load in the measured cycles is preserved as accurately as possible in the synthetic cycles. In the first phase, the overall average number of passengers in the bus during the new synthetic cycle is determined by sampling the number from the following conditional (bivariate) normal distribution (Publication I):

$$X_p|X_s = x_s \sim N\left(\mu_p + \frac{\sigma_p}{\sigma_s}\rho_{ps}(x_s - \mu_s), \left(1 - \rho_{ps}^2\right)\sigma_p^2\right) \tag{31}$$

where x_s is the number of stops at bus stops during the new synthetic cycle, μ_p is the overall average number of passengers in the bus during the measured cycles, μ_s is the mean number of stops at bus stops during a cycle in the measurements, σ_p is the standard deviation of the measured average passenger numbers, σ_s is the standard deviation of the measured number of stops at bus stops during a cycle, and ρ_{ps} is the Pearson correlation coefficient between the mean number of passengers and stops performed at bus stops during a cycle in the measurements.

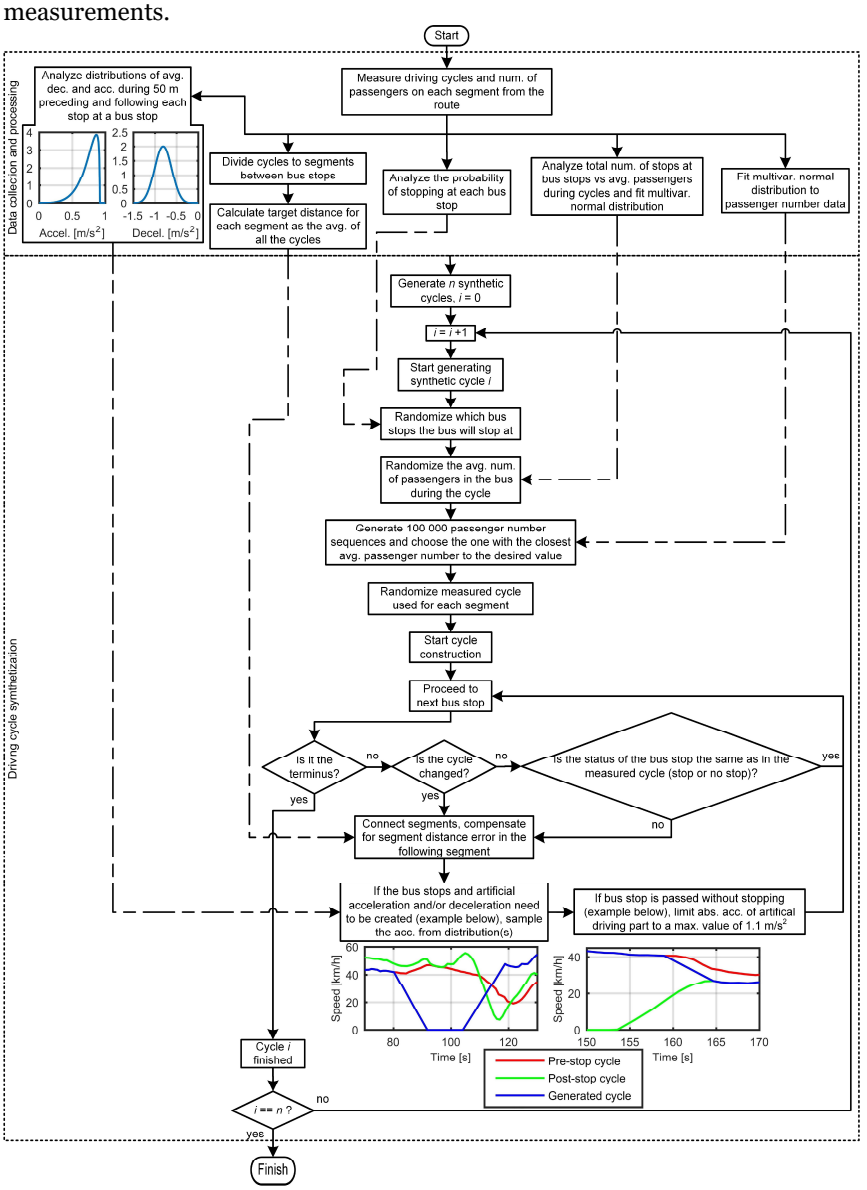

Figure 10. Flow chart of the driving cycle synthetization process (Publication II).

In the second phase, the number of passengers in the bus during each segment is sampled from a multivariate normal distribution. The covariance matrix of the distribution is defined as (Publication I):

$$\Sigma = \mathrm{cov}\left(\begin{bmatrix} n_{1,1} & \cdots & n_{1,M} \\ \vdots & \ddots & \vdots \\ n_{N,1} & \cdots & n_{N,M} \end{bmatrix}\right) \tag{32}$$

where N is the number of measured cycles, M is the number of segments, and $n_{i,j}$ is the amount of passengers in the bus on the j-th segment in the i-th cycle. In the case of Publication I, the drive from the terminus to the fast-charging station was included in the synthetic cycles and would always feature zero passengers in the bus. In Publication II, the drive to the fast-charging station was excluded due to the inclusion of various types of bus powertrains.

The number of passengers in the bus on each segment can then be sampled from a multivariate distribution defined by a vector of mean values of passengers in the bus during the measured cycles and by the covariance matrix presented in equation (32). 100000 passenger sequences are sampled, and the sequence with the overall average passenger number closest to the value determined in the first phase is selected. The passenger numbers must be limited between zero and a defined maximum occupancy and to stay constant between bus stops occurring. The validity of the driving cycle and passenger synthesis algorithm is examined in the Results chapter. An example of a synthetic Espoo bus line 11 cycle is shown in Figure 11.

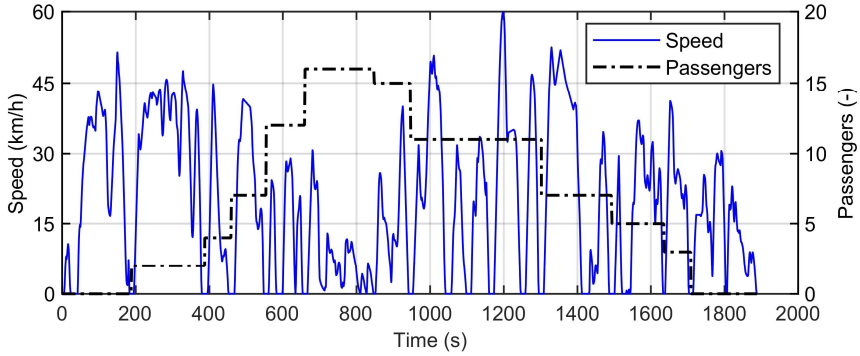

Figure 11. Example of a synthesized E11 driving cycle (Publication I).

3.4.2 Existing cycles

A collection of various existing bus driving cycles were used in Publications II and III (Table 8). In Publication II, the purpose was to compare the results acquired for a single route with the synthetic cycles to the results acquired from a more varied collection of cycles. In Publication III, the synthetic cycles were not used. All of the cycles listed in Table 8 were used in Publication II, and the cycles that are not denoted with light blue color were also used in Publication III. In both publications, the Braunschweig cycle, whose characteristic parameters were given in Table 2, was also used. Further descriptions of the cycles can be found in Publication II.

Table 8. Driving cycle characteristic parameters.

Parameter	B18	B51	E11B	H1	H2	H3	H24	H55	H550	H58	L05	L31	MAN	NYC	OCC	R36	RTE	TA25	TU03
Max. speed (km/h)	54.2	59.0	58.4	71.7	52.5	71.7	50.2	49.4	74.9	86.9	55.4	59.8	40.5	49.3	65.4	53.4	32.5	56.3	46.0
Avg. speed (km/h)	16.6	13.6	23.8	25.4	19.6	41.2	17.3	18.2	30.5	25.4	18.8	22.3	10.9	5.9	19.8	14.3	7.2	20.4	18.2
Avg. drv. spd (km/h)	22.4	19.7	27.5	33.2	26.5	47.9	20.4	22.9	35.5	32.6	25.2	27.1	16.4	15.9	24.4	20.0	13.6	24.2	22.2
Distance (km)	42.4	16.1	10.2	7.5	8.2	10.3	7.3	16.7	28.7	30.7	11.3	12.4	3.3	1.0	10.5	4.3	2.6	9.4	8.9
Stops per km	3.3	4.2	1.7	2.0	3.1	0.8	3.4	2.0	1.3	2.6	1.9	1.9	5.7	10.2	2.9	5.4	10.5	3.0	3.8
Duration (s)	9177	4283	1548	1066	1501	902	1529	3305	3384	4354	2165	1997	1089	600	1909	1084	1289	1667	1756
Total stop time (s)	2354	1336	412	249	394	125	234	668	472	961	549	355	363	377	355	309	606	262	315
Avg. stop duration (s)	16.8	19.4	11.4	15.6	15.2	13.9	9.0	19.6	12.4	12.0	23.9	14.2	18.2	34.3	11.5	12.9	21.6	9.0	9.0
Creep %	4.2	3.4	0.1	0.7	0.8	0.3	0.1	1.7	0.1	0.1	2.5	3.5	1.8	0.0	2.9	0.2	0.0	0.2	0.3
Cruise %	11.6	6.5	22.2	10.5	7.3	19.0	9.3	16.8	16.8	7.8	16.1	12.0	8.8	4.7	14.4	7.1	4.3	8.9	10.6
Idle %	26.6	32.4	13.3	24.2	26.8	13.9	15.9	20.4	14.1	22.4	26.1	18.6	34.3	65.3	19.6	28.5	56.9	16.3	18.5
Max. acc. (m/s^2)	1.87	1.93	1.60	1.50	1.50	1.42	2.83	0.99	2.03	1.93	1.52	1.81	2.00	2.76	1.81	1.87	1.69	2.84	4.10
Max. dec. (m/s^2)	2.21	1.98	1.90	2.33	2.33	1.94	3.82	1.53	2.86	3.14	1.70	2.14	2.49	2.04	2.29	2.10	2.26	4.44	3.95
Avg. acc. (m/s^2)	0.45	0.57	0.38	0.60	0.63	0.54	0.68	0.37	0.50	0.64	0.42	0.56	0.54	1.16	0.45	0.57	0.76	0.71	0.65
Avg. dec. (m/s^2)	0.51	0.60	0.39	0.60	0.62	0.56	0.73	0.33	0.50	0.78	0.39	0.46	0.70	0.67	0.66	0.55	1.07	0.77	0.68
Aggressiveness (m/s^2)	0.20	0.26	0.14	0.22	0.26	0.19	0.30	0.15	0.20	0.24	0.17	0.21	0.28	0.38	0.22	0.24	0.33	0.30	0.27

3.5 Statistical analysis

The Pearson correlation coefficient, which was employed in all three publications, describes the linear correlation between two variables x and y using the following equation [94]:

$$\rho_{xy} = \frac{\mathrm{cov}(x, y)}{\sigma_x \sigma_y} \tag{33}$$

where σ_i is the standard deviation of variable i. The coefficient can receive values ranging from -1 to 1 where -1 indicates total negative correlation, 0 indicates no correlation, and 1 indicates total positive correlation. In Publications I and II, the Pearson coefficient was used to quantify the correlation between various cycle parameters and the energy consumption of the bus models. In Publication III, it was employed to quantify the correlation between cycle parameters and the energy consumption reductions achieved with the various methods used.

In Publication I, the GSA method based on the Sobol approach was used to analyze the relative influence of the stop frequency and the passenger load on the energy consumption of the BEB. The method was implemented in MATLAB in [95].

One deficiency of the GSA method is that it assumes the input variables affecting the output variable to be uncorrelated. Hence, variance decomposition based on MLR was employed in Publication II to analyze the influence of the different cycle parameters on the energy consumption of the various bus powertrain topologies. The variance decomposition results can be found in Section 4.2. The method, which was presented by Xu and Gertner in [96], separates the portion of the effect of an input variable on the variance of the output variable that is not correlated with the effects of the other input variables. In other words, the contribution of an input variable to the output variable variance has an uncorrelated component as well as a correlated component that is caused by the interactions with other input variables, and the variance decomposition separates the two components according to the following equation [96]:

$$\hat{V}_i = \hat{V}_i^U + \hat{V}_i^C \tag{34}$$

where $\hat{V}_i$ is the total effect, $\hat{V}_i^U$ is the uncorrelated component, and $\hat{V}_i^C$ is the correlated component. The full description of the variance decomposition method can be found in [96]. In Publication II, the Pearson correlation coefficients between the cycle parameters and energy consumption were calculated first, and then the five parameters with the highest correlation with the consumption were selected along with the passenger load for further analysis with the variance decomposition. The number of cycle parameters utilized in the variance decomposition needed to be limited because the parameters are inherently connected to each other, and thus using too high a number of them would result in negligible uncorrelated components shown by the variance decomposition.

In Publication II, the statistical dispersion of the energy consumption of the different bus models was quantified using the coefficient of variation (CV),

which is calculated by dividing the standard deviation of the data with the mean value of the data. The coefficient of determination, denoted r^2, was employed in Publication III to assess the goodness of fit of the various efficiency map approximations used in the NMPC algorithm. The coefficient indicates the amount of variation in the output variable explained by the independent input variables in the regression model with the following equation [97]:

$$r^2 = 1 - \frac{SSE}{SST} \tag{35}$$

where SSE is the sum of squares of residuals, and SST is the total sum of squares.

3.6 Electric bus component choices for reducing consumption

In Publication III, four different component-choice-related methods for reducing the energy consumption of a BEB were compared with simulations. The methods included using:

1. a lightweight aluminum chassis instead of a steel chassis,
2. a low-height body to reduce aerodynamic drag,
3. premium class C tires instead of typical class E tires for reduced rolling resistance,
4. and an electric heat pump instead of a typical resistor-based heater to reduce the energy consumption of the HVAC system.

The methods were tested both individually using a proportional controller and all together along with NMPC driving optimization on 15 different driving cycles, discussed in Section 3.4, and in two ambient temperatures; -20 and 10 °C.

The parameter value changes caused by the different methods are shown in Table 9. The aluminum chassis was estimated to reduce the curb weight of the bus by approximately 15 % based on references [15], [76], and [80]. The reference aerodynamic drag value was set to represent a typical city bus featuring a ride height of 30 cm, height of 3.3 m, width of 2.55 m, and drag coefficient of 0.8 [78]. The drag values shown in Table 9 represent the product of the frontal area and drag coefficient. The lower body was approximated to have a frontal area of 6 m², and the aerodynamic drag coefficient is also known to reduce together with the frontal area [82], [83]. The tire classes based on rolling resistance values are presented in [84]. The HVAC power demand values for the two ambient temperature settings were determined using a graph found in reference [47]. The power demand reduction achieved using a heat pump instead of a resistance heater was estimated as 50 % based on references [16] and [17].

Table 9. Reference and reduced values of the BEB simulation model parameters (Publication III).

Parameter	Reference value	Reduced value
Bus curb weight (kg)	12350	10500
Aerodynamic drag (m²)	6.12	4.30
Rolling resistance coefficient	0.008	0.006
HVAC power at -10 °C (kW)	7.0	3.5
HVAC power at 20 °C (kW)	2.0	1.0

3.7 Model predictive control

In Publication III, the energy consumption reductions achievable with predictive driving were compared to those achievable with the component-related methods. Predictive driving was simulated with a nonlinear model predictive controller for driving optimization developed in MATLAB and Simulink. The Model Predictive Control Toolbox was used. The sequential quadratic programming (SQP) algorithm is utilized by the Simulink controller for solving the optimization problem. In this section, the electric bus model utilized by the NMPC algorithm is described as well as the cost function, constraints, and the different efficiency map approximations used by the algorithm.

The state-space model of the BEB is defined in the controller as (Publication III):

$$x(k+1) = \begin{cases} x_1(k) + x_2(k)T_s + a(k)T_s^2/2 \\ x_2(k) + a(k)T_s \end{cases} \tag{36}$$

where k is the discrete time instant, the distance travelled is the first state x_1, the second state x_2 is the speed of the vehicle, and T_s is the controller sample time. The model outputs are the same as the states. The acceleration is computed using equation (2) as (Publication III):

$$a(k) = \frac{F_w(k) - F_R(k)}{m + J_t/r_d^2}. \tag{37}$$

The resistive forces are calculated similarly as in equation (3) as:

$$F_R(k) = F_{rr}(k) + F_G(k) + F_d(k). \tag{38}$$

The rolling resistance term had to be modified slightly compared to equation (4) so as to keep the model continuous and continuously differentiable. The rolling resistance term is defined in the controller as:

$$F_{rr}(k) = mgf_{rr}\cos\big(\alpha(k)\big)\tanh(c_1 x_2(k)). \tag{39}$$

The hyperbolic tangent term drives the rolling resistance to zero when the speed falls to zero. The multiplier c_1 was defined as 5. The value was selected by examining how high the value could be set without making the model computationally slower. The gravitational force and the aerodynamic drag were calculated according to equations (5) and (6) as:

$$F_G(k) = mg\sin\big(\alpha(k)\big), \tag{40}$$

$$F_d(k) = \frac{1}{2}\rho c_D A\big(x_2(k)\big)^2. \tag{41}$$

The tractive force is calculated similar to equation (7) as (Publication III):

$$F_w(k) = u_1(k) i_g i_{fd} H_{dt,2} / r_d + u_2(k) \tag{42}$$

where u_1 is the torque of the electric motor, u_2 is the mechanical braking force, and $H_{dt,2}$ represents the drivetrain efficiency. The efficiency had to be defined differently compared to equation (8) in order to keep the model continuous and continuously differentiable. To that end, hyperbolic tangent was utilized with the following equation (Publication III):

$$H_{dt,2}\big(u_1(k)\big) = \frac{-\tanh\big(u_1(k)\big) + 1}{2\eta_g \eta_{fd}} + \frac{\big(\tanh\big(u_1(k)\big) + 1\big)\eta_g \eta_{fd}}{2} \tag{43}$$

which is an approximation of equation (8).

The inequality constraints are specified in the controller as (Publication III):

$$\begin{cases} x_2 \le v_{max} + c_{e1} e_s \\ x_2 \ge 0 \\ u_1 \le T_{EM,max} \\ u_1 \ge T_{EM,min} \\ u_2 \le 0 \\ u_2 \ge F_{B,max} \\ u_1 x_2 i_g i_{fd} / r_d \le P_{EM,max} \\ u_1 x_2 i_g i_{fd} / r_d \ge P_{EM,min} \\ x_1(k_c + p) \le d_{target} + c_{e2} e_s \\ x_1(k_c + p) \ge d_{target} - c_{e2} e_s \end{cases} \tag{44}$$

where v_{max} is the maximum speed currently allowed, $T_{EM,max}$ and $T_{EM,min}$ are the EM torque limits, $F_{B,max}$ is the maximum negative mechanical braking force, $P_{EM,max}$ and $P_{EM,min}$ are the EM power limits, k_c is the current instant, p is the prediction horizon length in number of time steps, d_{target} is the target distance, e_s is a slack variable used for softening the constraints, and c_{e1} and c_{e2} are slack coefficients. In Publication III, the 15 cycles described in Section 3.4.2 were employed. The cycles were split into segments between stops, with a stop being defined as any maneuver where the speed is zero for a minimum of two seconds. Each segment was given a maximum speed limit that was 5 km/h higher than the highest speed on that segment in the original cycle. The target distance was defined for the controller based on the driving cycles such that it would be equal to the distance travelled in the original cycle at the time instant of the end of the prediction horizon. However, the target distance would not be allowed to increase at the end of a segment until one second before the start of the next segment, thus ensuring stops would be handled properly. Hence, each segment driven with the NMPC would be virtually identical in terms of the total distance covered to the segment in the original cycle.

The cost function employed by the nonlinear model predictive controller is defined as (Publication III):

$$f = \sum_{k=1}^{p} \Big(c_{f1} H_{m'} u_1(k) \big(\omega_M(k) + \omega_M(k+1)\big)/2 + \big(c_{f2} u_2(k)\big)^2 + \big(c_{f3} x_2(k+1)\big)^2 + c_{f4} e_s^2 + \big(c_{f5}\big(u_1(k) - u_1(k-1)\big)\big)^2 + \big(c_{f6}\big(u_2(k) - u_2(k-1)\big)\big)^2 \Big) \quad (45)$$

where c_{fi} is the coefficient multiplying the i-th term and $H_{m'}$ represents the efficiency of the EM and inverter. The first term serves to minimize the energy consumption, while the second term gives a penalty for using the mechanical brakes. The third term further assists with the energy consumption reduction by helping to reduce the aggressiveness of the driving, which was given a mathematical definition in equation (1). In Publication II, it was shown that the energy consumption correlates strongly with the aggressiveness, and thus reducing the aggressiveness was desired to be incorporated into the cost function as well. The fourth term in the cost function penalizes for not adhering to the constraints. The more the constraints are violated, the more the value of the slack variable increases. The last two terms prevent rapid oscillations in the control inputs. The values of the coefficients in the cost function were chosen by first manually finding reasonable ranges and then sweeping through the ranges. The H58E cycle was employed for the sweep, as it is the most average of the 15 cycles in terms of aggressiveness, average speed, and stops per kilometer.

The variable $H_{m'}$ in equation (45) represents a smoothened approximation of equation (11), and it is defined as:

$$H_{m'} = \frac{\tanh\big(u_1(k)\big) + 1}{2\eta_{m'}(k)} - \frac{\tanh\big(u_1(k)\big) - 1}{2} \eta_{m'}(k) \quad (46)$$

where $\eta_{m'}$ is the efficiency of the electric motor and inverter according to the approximated efficiency map model. Tests showed that the hyperbolic tangent approximation reduced the computation time of the simulations by approximately 30 % compared to raising $\eta_{m'}$ to the power of the sign of the electric motor output torque. Additionally, torque is examined instead of power in equation (46), as the speed of the bus is assumed to never be negative. Hence, the signs of the power and torque would always be the same.

In order to study the effect of the efficiency map approximation type on the energy consumption reductions and computation times achieved, seven different approximation methods were tested. They are presented in (M1)-(M7).

$$\eta_{m'}(k) = \eta_{m,c} \quad (M1)$$

$$\eta_{m'}(k) = c_{00} + c_{10}\omega_M(k) + c_{01}|u_1(k)| \quad (M2)$$

$$\eta_{m'}(k) = c_{00} + c_{10}\omega_M(k) + c_{01}|u_1(k)| + c_{20}\omega_M(k)^2 + c_{11}\omega_M(k)|u_1(k)| + c_{02}u_1(k)^2 \quad (M3)$$

$$\eta_{m'}(k) = c_{00} + c_{10}\omega_M(k) + \cdots + c_{30}\omega_M(k)^3 + c_{21}\omega_M(k)^2|u_1(k)| + c_{12}\omega_M(k)u_1(k)^2 + c_{03}|u_1(k)|^3 \quad (M4)$$

$$\eta_{m'}(k) = c_1 + c_2\omega_M(k)|u_1(k)| \quad (M5)$$

$$\eta_{m'}(k) = c_1 + c_2 \tanh(c_3 \omega_M(k)|u_1(k)|) \quad \text{(M6)}$$

$$\eta_{m'}(k) = c_1 e^{c_2 \omega_M(k)|u_1(k)|} + c_3 e^{c_4 \omega_M(k)|u_1(k)|} \quad \text{(M7)}$$

In method (M1), the efficiency is assumed to be constant. This method maintains the lowest polynomial degree for the cost function and would thus be expected to be the most computationally-efficient. In methods (M2)-(M4), the efficiency map is approximated as a function of the torque and speed of the electric motor using first, second, and third-degree polynomial functions. The last three methods approximate the efficiency as a function of power output using linear (M5), hyperbolic tangent (M6), and exponential function (M7) fits. The actual efficiency maps as well as the approximations are presented in Figure 12 and Figure 13. The coefficients of determination of the different efficiency map approximations are presented in Table 10. It should also be noted that the NMPC does not include a battery model, so it does not account for the internal energy losses occurring in the battery. This was deemed acceptable because battery losses are low relative to the total losses of the vehicle, and the battery losses would be reduced anyway by the NMPC due to the reduced EM input power.

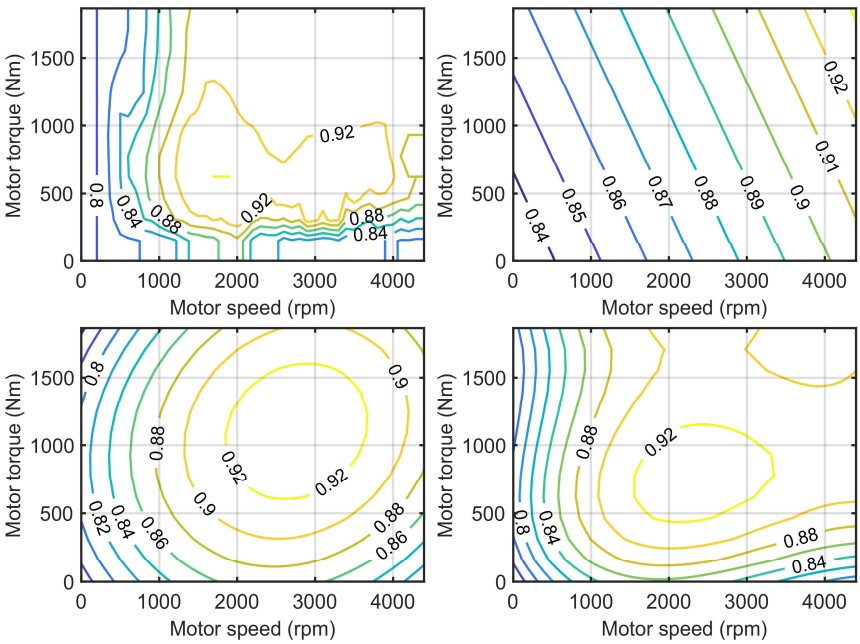

Figure 12. Actual efficiency map (top left) and the linear (M2, top right), second-degree polynomial (M3, bottom left), and third-degree polynomial (M4, bottom right) approximations used in the NMPC algorithm.

The controller sample time was set to 1 s for the simulation tests. The prediction and control horizons were set to 10 s. The ambient temperature was defined as -10 °C for all the NMPC tests. The default parameter values supplied by MATLAB were used for the SQP solver. An example of an NMPC-optimized driving cycle is presented in Figure 14. The NMPC was first tested using the reference bus parameter values shown in Table 9. After that, the NMPC was tested

together with all four component changes simultaneously in order to examine the total energy savings achievable when deploying all of the methods.

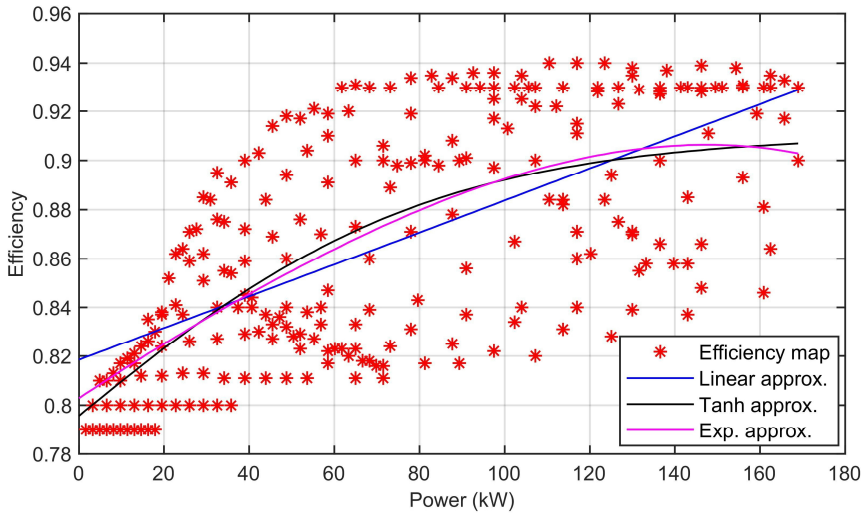

Figure 13. Linear (M5), hyperbolic tangent (M6), and exponential function (M7) efficiency map approximations.

Table 10. R^2 values of the efficiency map approximations.

	M2	M3	M4	M5	M6	M7
R^2	0.292	0.797	0.901	0.417	0.455	0.449

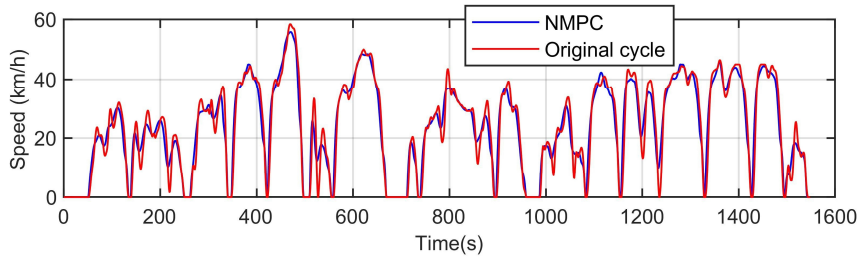

Figure 14. E11 cycle optimized with the NMPC algorithm using a 10-second horizon (Publication III).

4. Results

In this chapter, the most significant results obtained in the research are presented. Some results have been omitted, but they can be found in the publications.

4.1 Driving cycle synthesis and the effect of driving cycle uncertainty and passenger load on the energy consumption of a battery electric bus (Publication I)

The ability of the driving cycle synthesis method described in Section 3.4.1 to maintain the statistical properties of the original measurement data set was examined. The acceleration and speed distributions in the measured E11 cycles and 10000 synthetic E11 cycles are compared in Figure 15. Furthermore, other statistical properties are compared in Table 11.

Additionally, the ability of the algorithm to generate realistic passenger loads was examined. It was found that in 10000 synthetic cycles the Pearson correlation coefficient for the average passenger number and the average number of stops at bus stops during a cycle was 0.56. In the measurements, the Pearson coefficient was 0.60. In the synthetic cycles, the average number of passengers in the bus during a cycle was 5.8, and in the passenger measurements the value was 5.9. The highest mean number of passengers during a synthetic cycle was 14.33. The peak number of passengers at any point in the synthetic cycles was 38, while in the measurements the value was 29.

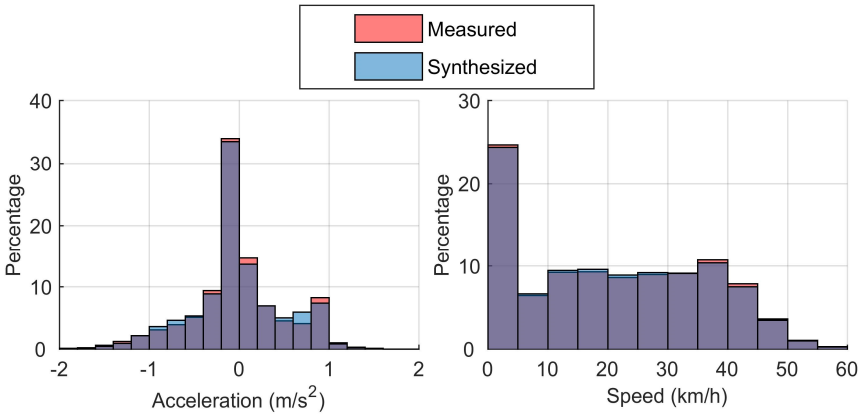

Figure 15. Histograms of the acceleration and speed in the 24 measured E11 cycles and 10000 synthesized E11 cycles (Publication I).

Table 11. Statistical parameter values of the measured and 10000 synthetic E11 cycles (Publication I).

Parameter	Measured cycles	Synthetic cycles
Average speed (km/h)	20.582	20.419
Avg. acceleration (m/s^2)	0.547	0.541
Avg. deceleration (m/s^2)	0.506	0.508
Avg. cycle duration (s)	1823	1837
Acceleration percentage	31.66 %	32.39 %
Deceleration percentage	34.15 %	34.37 %
Cruise percentage	15.63 %	15.11 %
Creep percentage	2.01 %	1.49 %
Idle percentage	16.55 %	16.65 %

The amount of synthetic cycles needed for acquiring representative energy consumption statistics for a route was examined by plotting the overall average energy consumption per cycle as a function of the number of simulated cycles (Figure 16). Furthermore, the mean and standard deviation of the consumption as a function of the number of cycles is presented in Table 12.

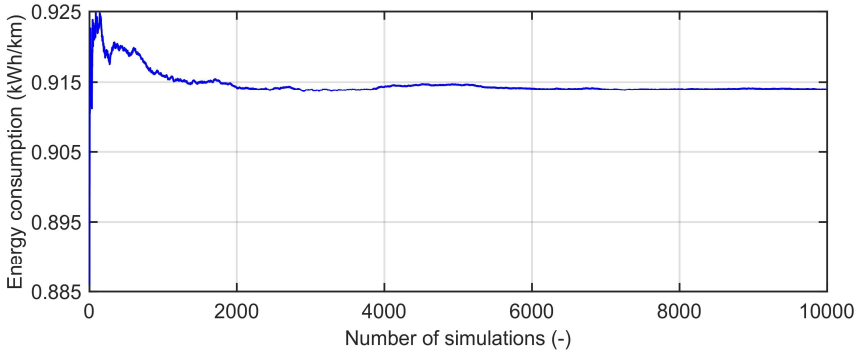

Figure 16. Overall mean energy consumption per cycle versus number of cycles (Publication I).

Table 12. Number of simulated synthesized cycles versus total mean consumption and standard deviation of consumption (adapted from Publication I).

Num. of cycles	Mean (kWh/km)	Std. dev. (kWh/km)
100	0.9239	0.0457
500	0.9194	0.0427
1000	0.9159	0.0423
2000	0.9142	0.0429
3000	0.9139	0.0425
5000	0.9146	0.0425
10000	0.9139	0.0431

A histogram of the energy consumption on the 10000 synthetically generated cycles is presented in Figure 17. The Pearson correlation coefficients between the energy consumption and various cycle parameters were also examined. In Table 13, the parameters are listed based on the absolute value from largest to smallest. The *number of stops* parameter includes all stops performed during a cycle, including at bus stops, traffic lights, and pedestrian crossings.

The GSA method discussed in Section 3.5 was utilized to analyze how much the stop frequency and average passenger load contributed to the energy consumption variations. The results showed that the variation in the stop frequency contributed 2.26 times more to the consumption than the passenger load variations did.

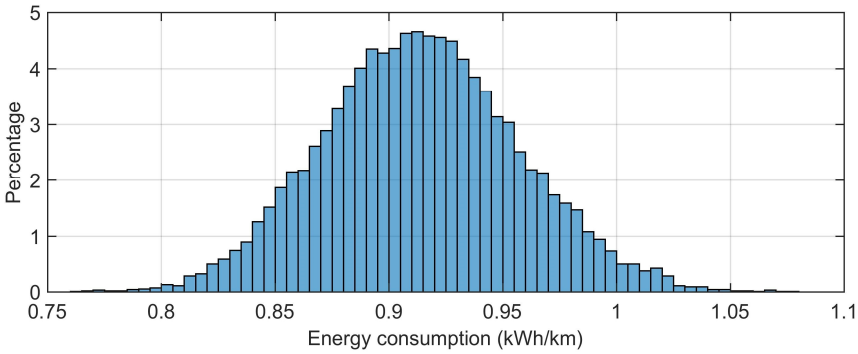

Figure 17. Histogram of the energy consumption on the 10000 synthetic E11 cycles (Publication I).

Table 13. Correlations between the energy consumption and driving cycle properties (Publication I).

Parameter	Pearson correlation coeff.
Number of stops	0.8053
Average speed	-0.7525
Number of stops at bus stops	0.7059
Cruise percentage	-0.6417
Average driving speed	-0.6271
Average passengers	0.6120
Average deceleration	-0.5954
Idle percentage	0.5658
Average acceleration	0.5574
Creep percentage	0.1720
Deceleration percentage	-0.1541
Acceleration percentage	-0.0560

4.2 Effect of driving cycle uncertainty and passenger load variations on the energy consumption of different types of city bus powertrain topologies (Publication II)

The histograms of the energy consumption with the six different bus models on the 3000 synthetic cycles are presented in Figure 18. The consumption statistics are listed in Table 14.

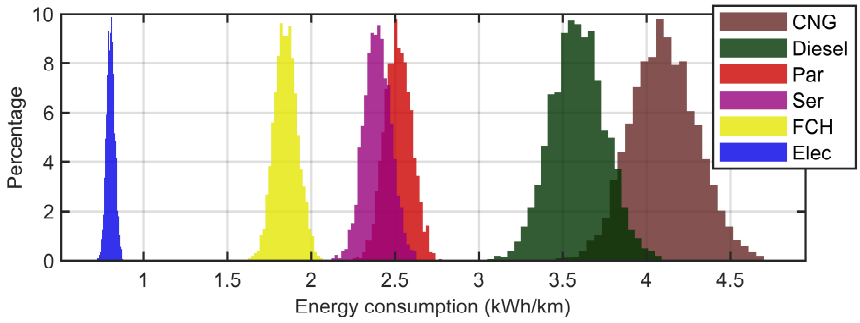

Figure 18. Energy consumption histograms for the six bus models on 3000 synthetic E11 cycles.

Table 14. Energy consumption statistics on the 3000 synthetic E11 driving cycles (Publication II).

Bus type	Mean (kWh/km)	Std. dev. (kWh/km)	CV (-)	Max. (kWh/km)	Min. (kWh/km)
CNG	4.103	0.197	0.048	4.744	3.340
Diesel	3.592	0.162	0.045	4.078	2.995
Parallel hybrid	2.517	0.081	0.032	2.776	2.199
Series hybrid	2.394	0.080	0.033	2.625	2.120
FCH	1.849	0.069	0.038	2.067	1.591
Electric	0.804	0.025	0.031	0.881	0.714

The Pearson correlation coefficients for the energy consumption and the cycle properties are shown in Table 15 where the properties have been listed based on the average absolute values from largest to smallest.

Table 15. Pearson correlation coefficients for energy consumption and cycle properties on the 3000 synthetic cycles (Publication II).

Parameter	CNG	DI	Par	Ser	FCH	Elec
Aggressiveness	0.789	0.857	0.772	0.810	0.806	0.791
Stops per km	0.827	0.779	0.812	0.755	0.797	0.799
Avg. speed	-0.828	-0.727	-0.803	-0.678	-0.778	-0.757
Cruise %	-0.697	-0.721	-0.672	-0.669	-0.701	-0.694
Total stop time	0.733	0.654	0.644	0.626	0.712	0.701
Avg. acc.	0.636	0.705	0.636	0.701	0.682	0.669
Avg. dec.	0.655	0.723	0.612	0.685	0.638	0.667
Avg. driving speed	-0.707	-0.601	-0.746	-0.576	-0.652	-0.630
Idle %	0.623	0.560	0.522	0.553	0.628	0.621
Avg. passengers	0.504	0.538	0.557	0.569	0.532	0.584
Creep %	0.218	0.195	0.247	0.181	0.240	0.222
Max. dec.	0.147	0.169	0.169	0.170	0.163	0.161
Max. speed	0.114	0.126	0.136	0.159	0.182	0.166
Avg. stop duration	0.163	0.104	0.061	0.090	0.165	0.147
Max. acc.	0.094	0.085	0.116	0.124	0.099	0.115

Based on Table 15, the five cycle parameters with the highest correlation with the energy consumption were chosen for the MLR-based variance decomposition analysis. Additionally, the average passenger load was included in the analysis. The results of the variance decomposition are presented in Figure 19 where the light brown bars denote the uncorrelated influence on the consumption.

The statistics of the energy consumption on the collection of existing cycles presented in Section 3.4.2 are shown in Table 16. The NYC cycle was left out of the analysis, so only 19 cycles were included in the analysis in the end. The reason the NYC cycle was excluded from the analysis was that the parallel hybrid model was not able to complete it without a significant reduction in the SOC of the battery. Furthermore, the B18 cycle needed to be run in two segments with the electric bus. The capacity of the battery pack was not high enough to complete the 42.4 km long cycle without one recharge en route.

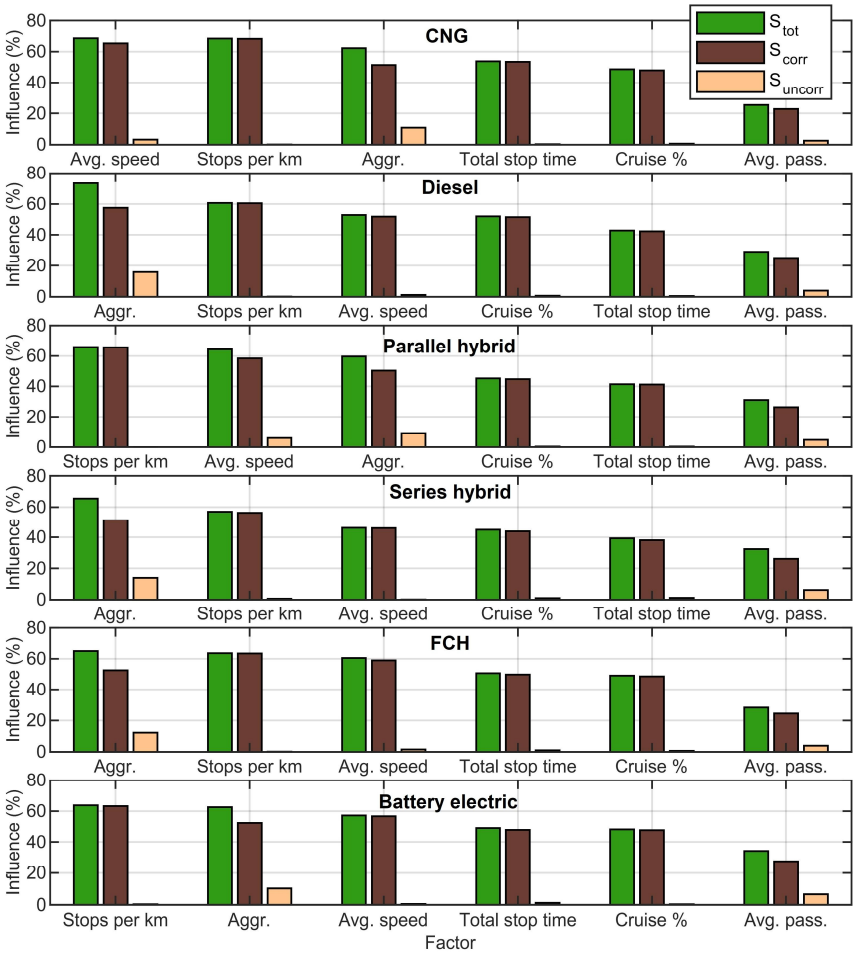

Figure 19. MLR-based variance decomposition analysis results for the synthetic E11 driving cycles (Publication II).

Table 16. Statistics of the energy consumption of the six bus models on the varied collection of existing bus driving cycles (Publication II).

Bus type	Mean (kWh/km)	Std. dev. (kWh/km)	CV (-)	Max. (kWh/km)	Min. (kWh/km)
CNG	4.932	1.267	0.257	8.993	3.516
Diesel	4.199	0.913	0.218	7.018	3.041
Parallel hybrid	2.967	0.573	0.193	4.689	2.291
Series hybrid	2.802	0.420	0.150	4.098	2.193
FCH	2.240	0.367	0.164	3.349	1.707
Electric	0.929	0.131	0.141	1.355	0.742

The Pearson correlation coefficients between the consumption and the cycle properties on the collection of existing cycles are presented in Table 17. The variance decomposition analysis, shown in Figure 20, was conducted by selecting the top five parameters in Table 17.

Table 17. Pearson correlation coefficients for energy consumption and cycle properties on the existing bus driving cycles presented in Section 3.4.2 (excluding the NYC cycle) (Publication II).

Parameter	CNG	DI	Parallel	Series	FCH	Electric
Stops per km	0.970	0.954	0.933	0.879	0.932	0.889
Aggressiveness	0.830	0.876	0.900	0.916	0.871	0.845
Cruise %	-0.818	-0.834	-0.837	-0.809	-0.836	-0.759
Avg. dec.	0.718	0.769	0.811	0.880	0.782	0.820
Idle %	0.842	0.808	0.753	0.706	0.821	0.775
Avg. acc.	0.629	0.686	0.666	0.765	0.654	0.676
Avg. speed	-0.771	-0.746	-0.702	-0.548	-0.676	-0.519
Avg. drv. speed	-0.789	-0.770	-0.575	-0.455	-0.578	-0.408
Max. speed	-0.677	-0.645	-0.621	-0.478	-0.549	-0.450
Creep %	-0.258	-0.294	-0.337	-0.425	-0.329	-0.410
Avg. stop duration	0.352	0.293	0.237	0.177	0.333	0.297
Max. acc.	0.174	0.238	0.289	0.289	0.188	0.156
Max. dec.	0.118	0.198	0.242	0.312	0.164	0.176
Total stop time	0.132	0.124	0.067	0.034	0.131	0.077

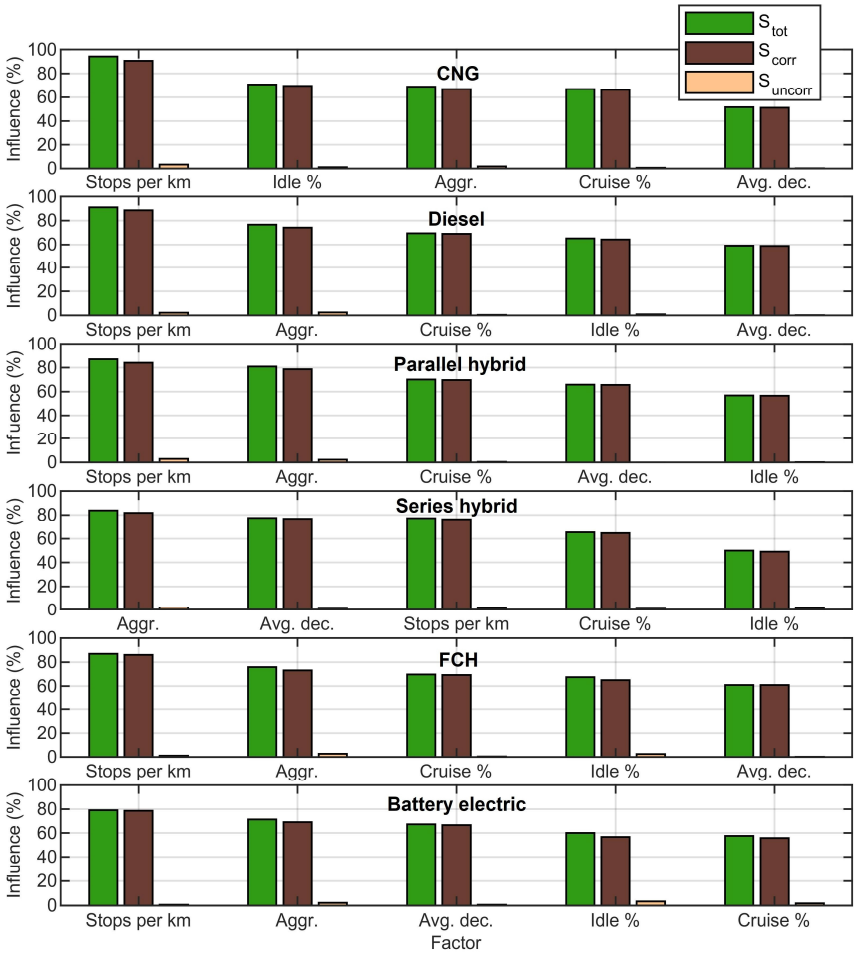

Figure 20. MLR-based variance decomposition analysis results for the collection of existing cycles (Publication II).

4.3 Effect of different energy consumption reduction methods and predictive driving on the energy consumption of a battery electric city bus (Publication III)

Figure 21 presents the energy losses on the 15 cycles described in Section 3.4.2 using the reference parameter values and the proportional controller. The losses in both ambient temperatures are included in the figure. The statistics of the losses are further detailed in Table 18. The powertrain losses were considered to include the losses of the electric motor, inverter, and gear reductions.

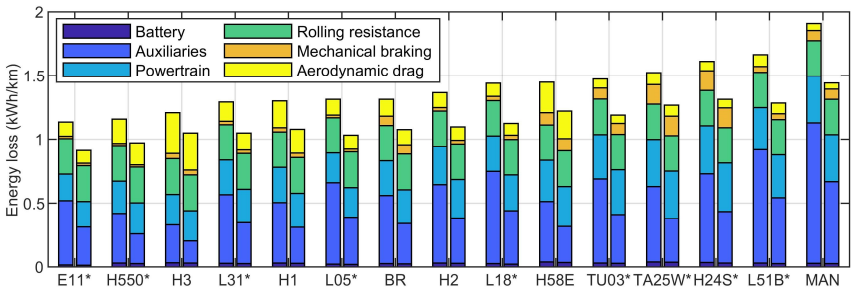

Figure 21. Energy loss distributions with the reference parameter values. The left side bars are the losses at -10 °C and the right-side bars at 20 °C. The cycles denoted in the x-axis label with a star featured a road grade profile (Publication III).

Table 18. Energy loss distributions for each loss category with the reference parameters. The upper value is for -10 °C and the lower value for 20 °C. RR stands for rolling resistance.

	Total	Battery	Auxiliaries	Powertrain	RR	Brakes	Drag
Mean	1407.1	28.6	607.8	295.5	278.2	60.3	140.1
(Wh/km)	1363.3	26.1	354.5	294.5	278.2	60.4	125.8
Std. dev.	206.3	5.8	197.3	54.1	0.07	46.0	73.0
(Wh/km)	141.9	5.6	115.1	54.5	0.07	46.1	65.5
Max.	1908.7	38.5	1099.4	376.2	278.3	155.8	323.0
(Wh/km)	1442.1	36.0	641.3	375.9	278.3	156.1	290.1
Min.	1130.7	15.0	292.8	207.2	278.0	16.5	55.9
(Wh/km)	906.9	13.2	170.7	206.5	278.0	16.6	50.2

The energy consumption reductions achieved with the four component-choice-related methods discussed in Section 3.6 are presented in Figure 22. The mean energy consumption reductions achieved with the aluminum chassis, low-drag body profile, low-rolling-resistance class C tires, and electric heat pump were 98, 45, 73, and 179 Wh/km at -10 °C. At 20 °C, the energy savings provided by the low-drag body and heat pump were 40 Wh/km and 51 Wh/km. The temperature had no effect on the consumption reductions yielded by the aluminum chassis and class C tires.

The energy consumption reductions achieved with the NMPC driving optimization are displayed in Figure 23 where the electric motor and inverter efficiency map approximations described in Section 3.7 are compared using boxplots. The average consumption reduction was 9.3 % - 9.8 % depending on the efficiency map approximation. Method (M3) achieved the highest energy savings with an average value of 138 Wh/km, and the lowest savings were provided by method (M5) with an average consumption reduction of 131 Wh/km. Of the efficiency

map models, method (M1) achieved the highest simulation speeds, performing on average at 1.42 times real-time. For comparison, the simulation model performed on average approximately 350 times faster than real-time when utilizing the regular proportional controller. A desktop PC with an Intel Xeon E3-1231 v3 @ 3.4 GHz processor was utilized for running the simulations.

The energy losses were examined more closely with the method (M1) simulations. The powertrain losses were reduced on average by 24 % or 74 Wh/km on the 15 cycles, which accounted for the majority of the energy savings. Mechanical braking loss reductions were also significant, as the losses were cut by 16 to 77 % depending on the cycle. The variation in the mechanical braking losses was reduced substantially with the NMPC optimization, as the highest braking losses were 5.0 times as high as those on the cycle with the lowest brake losses, while in the original cycles the factor was 10.4. Battery losses were cut by 23 to 52 % and drag losses by 4 to 28 %. The total energy consumption reduction varied between 5.4 and 17.4 %.

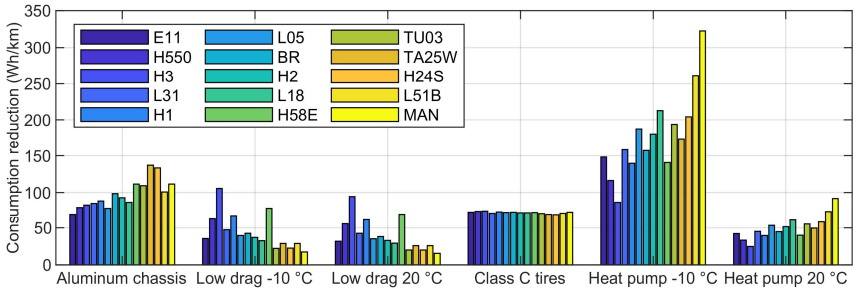

Figure 22. Effect of the different energy consumption reduction methods on the 15 driving cycles with the proportional controller (Publication III).

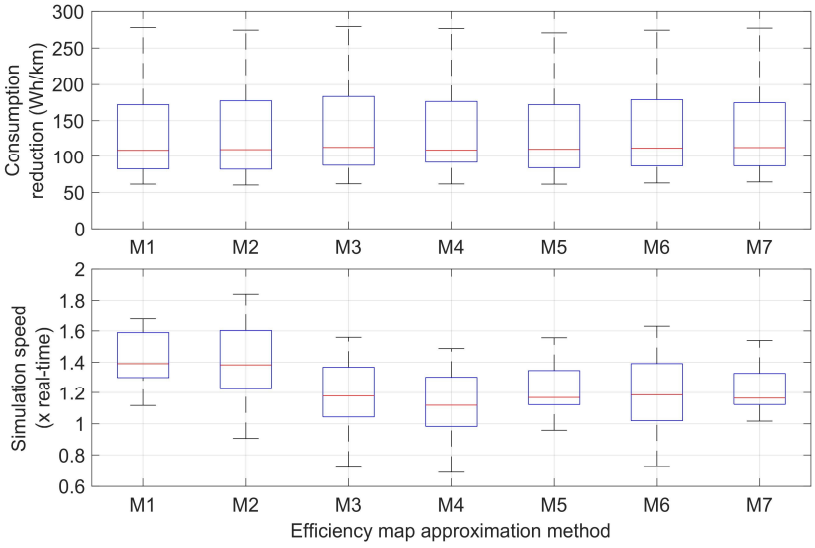

Figure 23. Effect of the efficiency map approximation method on the consumption reductions and simulation model computational speed with a 10-second horizon on the 15 cycles (Publication III).

The energy losses on the 15 cycles when using all four component-choice-related methods for reducing the consumption as well as the NMPC driving optimization are depicted in Figure 24. Further statistics are provided in Table 19.

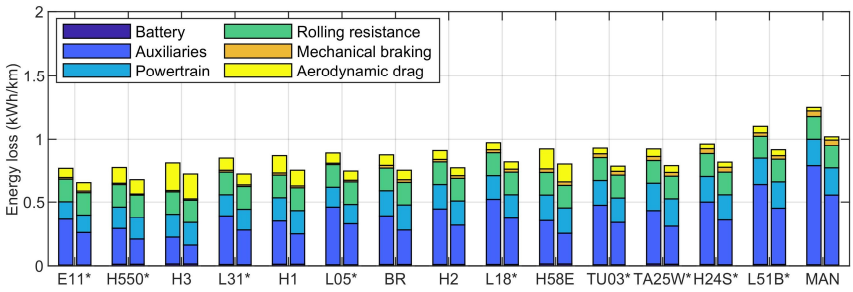

Figure 24. Energy loss distributions with all the component-choice-related methods as well as NMPC in use. The prediction and control horizon length of the NMPC was 10 s. The left side bars are the losses at -10 °C and the right-side bars at 20 °C. The cycles denoted in the x-axis label with a star featured a road grade profile (Publication III).

Table 19. Energy loss distributions for each loss category when utilizing all of the component-related methods as well as NMPC with 10-second prediction and control horizons. The upper value is for -10 °C and the lower value for 20 °C. RR stands for rolling resistance.

	Total	Battery	Auxiliaries	Powertrain	RR	Brakes	Drag
Mean	914.9	10.9	429.6	187.5	178.4	22.6	87.9
(Wh/km)	778.0	10.2	303.3	186.6	178.4	22.6	78.9
Std. dev.	125.2	2.7	139.7	22.3	0.03	10.9	50.9
(Wh/km)	90.8	2.6	98.6	22.4	0.03	10.9	45.7
Max.	1250.3	15.8	777.2	217.5	178.5	45.2	217.1
(Wh/km)	1017.9	14.9	548.6	216.6	178.5	45.2	195.0
Min.	762.5	6.3	206.0	138.4	178.4	9.4	27.3
(Wh/km)	649.2	5.7	145.4	137.9	178.4	9.4	24.5

5. Discussion

The first research question was how one could generate a large quantity of realistic driving cycles and passenger numbers for a single bus route based on a handful of measurements from the route. The speed and acceleration histograms in Figure 15 as well as the statistical properties shown in Table 11 indicate that the novel cycle synthesis method described in Section 3.4.1 is capable of maintaining the statistical properties of the original measured cycles with a high degree of accuracy. The mean difference in the bin sizes of the acceleration histogram was only 0.47 %-points and 0.21 %-points in the speed histogram. Furthermore, as discussed in Section 4.1, the statistical properties of the synthetically generated passenger numbers were close to those of the original measurements. The difference between the mean number of passengers in the synthetic and measured cycles was only approximately two percent. The results also showed that the average passenger load correlated with the number of stops at bus stops in a similar fashion as in the measured cycles. This similarity can be inferred from the difference in the Pearson correlation coefficients between the synthetic cycles and measurements, which was only 0.04. Hence, it can be stated that the novel driving cycle and passenger load synthetization algorithm provides an answer for the first research question. In addition, Figure 16 and Table 12 demonstrate that a relatively low number of cycles needs to be simulated in order to acquire a representative energy consumption distribution for a route. After 500 simulated cycles, the overall mean consumption was 0.6 % higher than after 10000 cycles. After 1000 cycles, the difference was merely 0.2 %. The standard deviation of the consumption stayed within two percent of the final value after 500 cycles.

The second and third research questions were both studied in the first two publications. The energy consumption distributions acquired in Publication II with both the synthetic cycles (Figure 18 and Table 14) as well as the cycles discussed in Section 3.4.2 (Table 16) indicated that BEBs are the most robust against driving cycle and passenger load uncertainty of all the compared bus types, as the coefficient of variation was the lowest for the BEB in both cases. The CNG bus had the highest consumption and highest coefficient of variation in both tests, and the diesel bus also performed significantly worse than the hybrid models. The high consumption and sensitivity of the consumption to cycle variations is explained by the lack of regenerative braking. Out of the hybrid buses, the fuel cell hybrid had the highest coefficient of variation in the synthetic cycles. On the collection of different existing cycles, the parallel hybrid had a significantly higher coefficient of variation of the consumption compared to the

other two hybrid models. On further examination, it was noticed that the consumption of the parallel hybrid increased significantly more compared to the other hybrid models when the stop frequency increased beyond 2.5 stops per km and the aggressiveness beyond 0.23 m/s^2. The phenomenon was partially caused by the lower-powered electric motor featured in the parallel hybrid, which limited the regenerative braking capability of the powertrain. The results demonstrate that a parallel hybrid powertrain can provide better performance than series hybrid on an appropriate route, but on routes with aggressive stop-and-go type driving the parallel hybrid configuration may prove inefficient. It is thus strongly recommended for transport authorities to be attentive to which kinds of routes parallel hybrid buses are deployed on. The result also demonstrates the importance of optimizing the braking maneuvers particularly with parallel hybrid buses that feature less powerful electric motors.

The results in both Publications I and II indicated that the stop frequency highly influences the energy consumption of city buses. In addition, the results in Publication II showed that the aggressiveness, which was defined in equation (1), describes the energy demand of a driving cycle well. The aggressiveness had the highest correlation with the energy consumption on the synthetic cycles, as was demonstrated in Table 15. Furthermore, the variance decomposition analysis of the synthetic cycles showed the aggressiveness to have the highest uncorrelated influence on the energy consumption. The aggressiveness greatly affecting the energy consumption indicates that it is highly important to limit the accelerations performed at high speeds with city buses in order to reduce the energy consumption regardless of the powertrain type.

In the case of the conventional bus types, the aggressiveness had higher uncorrelated influence on the energy consumption of the diesel bus than on that of the CNG bus. The phenomenon can be explained by the fact that the diesel engine featured a more consistent efficiency map in the operating region, which is typically the case between diesel and CNG engines. Hence, the efficiency of the CNG engine would generally increase more when the aggressiveness of the driving increases. It is nonetheless an interesting observation, as the CNG powertrain is heavier, which should in turn make the CNG bus more sensitive to changes in the aggressiveness. Of all the buses, the energy consumption of the parallel hybrid was the least sensitive to the aggressiveness in the synthesized cycles based on the variance decomposition results in Figure 19. The result is likely explained by the fact that the internal combustion engine is coupled with the driven wheels in the parallel hybrid, and hence its efficiency would typically increase with more aggressive acceleration maneuvers, slightly offsetting the increased losses. With the other two hybrid powertrain types as well as the fully electric powertrain, only the electric motor is coupled with the driven wheels, and electric motors tend to have significantly more consistent efficiency maps than internal combustion engines.

In the simulations where the existing cycles described in Section 3.4.2 were used, the stop frequency had the highest correlation with the consumption, and the aggressiveness had the second highest correlation (Table 17). The average

deceleration also had a slightly higher correlation with the consumption compared to the single route simulations, particularly with the hybrid and electric bus models. This was likely due to some of the cycles featuring more deceleration maneuvers where mechanical braking was required in addition to the regenerative braking. The variance decomposition analysis (Figure 20) showed less uncorrelated influence for the aggressiveness compared to the synthetic cycle simulations for all the bus models. This was mostly because there was more variation in the other aspects of the cycles compared to the single route simulations, which meant the aggressiveness also correlated more with the other cycle properties. In addition, the average deceleration, which had a high amount of correlation with the aggressiveness (-0.90), was included in the variance decomposition in the case of the existing cycles. However, the relative trends between the different bus models were still similar. The aggressiveness had less uncorrelated influence on the consumption of the CNG bus compared to the diesel bus. Additionally, there was more uncorrelated influence on the consumption of the FCH bus than on the consumption of the BEB. It is also worth noting that the Pearson correlation coefficient for the aggressiveness and the energy consumption, as well as for the average deceleration and consumption, was lower with the parallel hybrid than with the series hybrid even though it was mentioned earlier that the performance of the parallel hybrid deteriorated significantly beyond certain aggressiveness values. This discrepancy is likely a result of the Pearson coefficient being a measure of linear correlation. At high aggressiveness and average deceleration values, the effect of the aggressiveness and average deceleration on the consumption appeared to be exponential.

The variance decomposition analysis of the synthetic cycle simulation results, presented in Figure 19, showed the passenger load variations to have had less uncorrelated influence on the energy consumption of the conventional buses compared to the energy consumption of the hybrid models and the BEB. The passenger load had less effect on the energy consumption of the diesel and CNG buses compared to that of the electrified models because the cycle properties had comparatively more influence due to the lower and more inconsistent powertrain efficiency as well as the lack of regenerative braking. Overall, the passenger load variations had significantly less effect on the energy consumption compared with the driving cycle uncertainty.

Research questions four, five, and six were focused on in Publication III. The energy loss distributions with the reference values (Figure 21 and Table 18) showed that the auxiliaries were the single most significant cause of energy usage. In cold conditions, the auxiliaries accounted for nearly half of the energy losses on average. Consequently, the electric heat pump achieved the highest consumption reductions of the four component-choice-related methods listed in Section 3.6 in the -10 °C simulations, as can be seen in Figure 22. In the warmer conditions, the energy savings were less than one third of the savings achieved in the cold conditions. Previous publications have shown that the HVAC power requirement is particularly low in ambient temperatures ranging from 5 to 20 °C [47]. The energy consumption reductions provided by the electric heat pump were also highly dependent on the driving cycle. The slower the

average speed of the cycle was, the more advantageous the heat pump was relative to the other methods. Hence, an electric heat pump is recommended to be used particularly on low-speed routes and in regions with a cold climate.

While the energy savings achieved by the heat pump were highly dependent on both the temperature and the cycle, the class C tires provided consistent energy use reductions with minimal variations. The robustness is caused by the fact that the rolling resistance is only affected by the road grade, as can be seen in equation (4). While the aluminum chassis also provided relatively consistent energy consumption reductions, which were even higher than those achieved with the low-rolling-resistance tires, the energy savings did correlate strongly with the aggressiveness of the cycle. The Pearson correlation coefficient for the aggressiveness of the cycle and the consumption reduction provided by the aluminum chassis was 0.94. The low-height body achieved the lowest consumption reductions in both temperatures. The results demonstrated that the lower drag is only notably beneficial on higher-speed routes, and even then it is only slightly more effective than the low-rolling-resistance tires.

The NMPC simulation results showed that the electric motor and inverter efficiency map approximation method used in the problem formulation had only a marginal effect on the energy consumption. However, the computational efficiency was significantly affected. While the polynomial approximation (M3) produced the highest energy consumption reductions, the results clearly indicated that the assumption of constant efficiency (M1) is the optimal way to approximate the efficiency, as it provided the highest and most consistent computational speeds. Overall, it can be stated that the driving optimization problem formulation, presented in Section 3.7, in combination with the constant efficiency approximation provides an answer for research question five. For research question six, the results indicated that energy savings of approximately 10 % could be achieved with predictive driving. Additionally, the high reduction in mechanical braking losses in the NMPC simulations indicated the importance of optimizing the braking maneuvers with electric buses. Attention should be paid to providing bus drivers with assistance systems as well as intuitive and easy-to-use controls for maximizing the regenerative braking.

Finally, the results of the simulations where all of the component-choice methods as well as the NMPC were employed indicated that there is substantial room to reduce the energy consumption of city buses. In cold conditions, the consumption was reduced by an average of 492 Wh/km or 35 %. The average reduction in the warm conditions was 358 Wh/km or 31 %.

However, the conducted research also featured several limitations. Firstly, the driving cycles that were used as the basis of the cycle synthesis in Publications I and II were only recorded during winter months. It is not known how much the driving cycles would vary on that particular route depending on the time of year. Furthermore, the cycle synthesis simulations were only conducted for a single route, and it is thus unknown how the results would relate to those acquired from different kinds of bus routes. Additionally, the power demand of the diesel heater was not included in the BEB simulation model in Publication I, as measurement data was not available from the electric bus equipped with the IoT data

acquisition system. Thus, in reality the energy consumption of the bus would be significantly higher in cold conditions.

The cycle synthesis algorithm used in the first two publications could also be improved in several ways. Firstly, the created artificial acceleration and deceleration maneuvers featured constant acceleration values. This was considered to be acceptable due to the examined E11 route, as the low speeds would ensure that the power demand would stay reasonable during the artificial accelerations and decelerations. As was shown in Section 4.1, the synthesis algorithm did maintain the statistical properties of the original measurements well. Nonetheless, for routes with higher speeds, the acceleration maneuvers should be created in such a way that the acceleration at higher speeds is restricted so as to limit the power demand. Additionally, on routes where significant differences in the driving cycles occur based on the time of day, cycles should be separately synthesized for rush hours and non-rush hours. On the examined route, the time of day appeared to make minimal difference to the driving maneuvers, and hence it was deemed acceptable to mix segments from different hours.

In Publications II and III, the number of existing driving cycles, discussed in Section 3.4.2, was limited. A higher number of cycles would provide more thorough results. Although the energy consumption results of Publication II should be relatively generalizable due to the nature in which the bus models were parametrized, it would still be beneficial to feature variations in the specifications of the bus types in order to acquire broader results. Furthermore, non-plug-in type buses should be compared as well. It is also interesting to note that the different types of simulation models of battery electric buses used in Publications I and II produced slightly different results. The consumption was higher on average in Publication I although that is explained mostly by the higher auxiliary power demand. However, the coefficient of variation of the consumption was also higher in Publication I.

Another consideration is that while the simulated bus models used in Publication II were designed to be generic representations of the bus types examined, the designs could be suboptimal. The degree to which the optimality, or lack thereof, of the models affected the results is unknown. Additionally, the control logic used by Autonomie to operate the hybrid systems influenced the optimality of the powertrains, but the extent of the influence is unknown, as it was not analyzed. Hence, future work is needed to analyze the influence of component and control logic variations on the energy consumption results. In addition, further research should be conducted into examining the performances of different types of models to understand how to best produce simulation models that have a realistic amount of sensitivity to different types of uncertainty.

The statistical analysis methods used in the research featured one significant limitation in that they only considered the linear correlations between the parameters. Additionally, the NMPC driving algorithm in Publication III used the existing cycles to acquire the target distance. If the algorithm was to be used in a real application, a method for determining the target distance would have to be developed as well as incorporating the ability to follow a vehicle safely. Nonetheless, the way the NMPC was implemented in this research was deemed to

provide a decent approximation of predictive driving because the maneuvers were constrained by the characteristics of the original cycles.

6. Conclusion

In this doctoral dissertation, the sensitivity of the energy consumption of city buses to driving cycle uncertainty and passenger load variations was investigated. Additionally, the effectiveness of different methods for reducing the energy consumption of city buses were compared.

A novel driving cycle synthetization algorithm was developed. The algorithm can produce a large number of varying realistic cycles for a single bus route based on limited measurement data from the route in question. Additionally, the algorithm generates varying passenger numbers for each synthetic cycle based on passenger measurements from the route. Driving cycles were collected from a suburban route in Espoo, Finland in order to use them as the basis of the synthetization process. Ten thousand synthetic cycles were generated, and their statistical properties were compared to those of the measured cycles. The results indicated that the synthetization algorithm maintains the statistical properties of the original measured cycles with good precision.

The sensitivities of different types of city bus powertrain topologies to driving cycle uncertainty and passenger load variations were compared with bus simulation models using 3000 synthetic cycles as well as a collection of existing cycles used in previous studies. The compared models included a compressed natural gas, diesel, parallel hybrid, series hybrid, hydrogen fuel cell hybrid, and battery electric bus. Compared to the diesel bus, the CNG bus had a higher statistical dispersion of the energy consumption. The electric bus was the most robust against the driving cycle and passenger load uncertainty. The parallel hybrid had a lower consumption dispersion on the synthetic cycles compared to the series hybrid, but on the collection of existing cycles the parallel hybrid was significantly less robust against the driving cycle uncertainty. Hence, the result indicated that parallel hybrid buses can perform well on routes suited to them, but they are also susceptible to poor performance on congested routes with aggressive stop-and-go type driving. Of the hybrid models, the fuel cell hybrid had the lowest average consumption although the statistical dispersion of the consumption was higher than that of the series hybrid model.

The aggressiveness of the driving was given a mathematical definition so as to compare its influence on the consumption of the six different bus types. The results demonstrated that the aggressiveness value is a good indicator of the energy demand of a driving cycle, as the aggressiveness correlated the strongest with the consumption of all the cycle parameters along with the stop frequency. In addition, the high influence of the aggressiveness on the consumption with

all the bus models implies that accelerations at high speeds should be limited regardless of the powertrain type in order to reduce energy consumption.

Multiple-linear-regression-based variance decomposition was used to further examine the effect of the aggressiveness on the consumption. The results indicated that diesel buses are the most sensitive to the aggressiveness of the driving. It is therefore of high importance to provide assistance systems and coaching especially for diesel bus drivers to minimize the aggressiveness of their driving styles. The parallel hybrid bus was the least sensitive to the aggressiveness on the synthetic cycles, showing that it can be a robust choice when used on a suitable route. The battery electric bus was less sensitive to the aggressiveness than the hydrogen fuel cell hybrid, mainly due to the lower mass.

The presented research indicated that passenger load is not as influential to the energy consumption of city buses as the driving cycle uncertainty. The conventional bus models were less affected by the passenger load compared with the hybrid and battery electric bus models.

Four key component-choice-related methods for reducing the energy consumption of a battery electric bus were compared. The comparison included using a lightweight aluminum chassis instead of a steel chassis, employing a low-height body for reduced aerodynamic drag, using low-rolling-resistance class C tires instead of typical class E tires, and utilizing an electric heat pump instead of a conventional heater. The consumption reduction studies showed that using an electric heat pump instead of a conventional heater has the highest energy savings potential. However, the effectiveness strongly depends on the ambient temperature and driving cycle. The electric heat pump was shown to be at its most advantageous on low-speed routes and cold conditions. The low-rolling-resistance tires produced the most robust consumption reductions although using an aluminum chassis instead of steel chassis was more effective overall. Using a low-height body for reduced aerodynamic drag was an effective means for reducing the consumption only on the highest-speed cycles.

The predictive driving studies demonstrated that the way the efficiency map of the electric motor and inverter is approximated in the NMPC problem formulation makes minimal difference to the energy consumption, but it has a significant effect on the computational speed of the controller. Hence, it is recommended to approximate the efficiency as constant. Overall, the energy savings achieved with the predictive driving were higher than those produced by the component-related methods except for the electric heat pump in cold conditions. Using all of the presented methods together reduced the consumption by more than 30 % in both the cold and warm conditions, demonstrating that there is much room to reduce the energy consumption of city buses.

There are many directions that the topics covered in this thesis could be taken in the future. The cycle synthesis concept could be improved upon, for example by creating the artificial driving portions in a more complex way such that the accelerations are not constant. Generally, there is still room for improvement in how well the synthesis method maintains the statistical properties of the original measurements. Various different routes could also be compared using the

cycle synthesis in order to get a more complete picture of the consumption fluctuations on different route types. More powertrain types and varying specifications could be compared as well. The influence of variations in the control logic of the hybrid systems on the energy consumption results could be investigated. Powertrain and control logic optimization algorithms could be developed for the purposes of energy consumption uncertainty analyses. More advanced statistical analysis methods could be employed to account for the nonlinear correlations between the different cycle properties and the consumption. The effect of different ambient temperatures on the energy consumption influence of driving cycle uncertainty and passenger load variations with different bus types could also be examined. With the consumption reduction methods, the lifecycle costs of the different methods should be investigated in detail. Different routes and conditions should be considered in the analysis as well. Additionally, further work is required on the NMPC algorithm to make it usable in real applications. The target distance needs to be calculated dynamically, and vehicle-following should be implemented as well. In addition, the sensitivity of the control algorithm to various sources of uncertainty should be tested.

References

[1] The Intergovernmental Panel on Climate Change, “Climate Change 2014 Synthesis Report,” Geneva, Switzerland, 2015.

[2] “Sources of Greenhouse Gas Emissions,” *United States Environmental Protection Agency*, 2018. [Online]. Available: https://www.epa.gov/ghgemissions/sources-greenhouse-gas-emissions. [Accessed: 21-Feb-2019].

[3] “Greenhouse gas emissions from transport,” *European Environment Agency*, 2018. [Online]. Available: https://www.eea.europa.eu/data-and-maps/indicators/transport-emissions-of-greenhouse-gases/transport-emissions-of-greenhouse-gases-11. [Accessed: 21-Feb-2019].

[4] M. Rogge, S. Wollny, and D. U. Sauer, “Fast Charging Battery Buses for the Electrification of Urban Public Transport—A Feasibility Study Focusing on Charging Infrastructure and Energy Storage Requirements,” *Energies*, vol. 8, no. 5, pp. 4587–4606, 2015.

[5] International Association of Public Transport, “Public Transport Trends 2017,” Brussels, Belgium, 2017.

[6] M. Keegan, “Shenzhen’s silent revolution: world’s first fully electric bus fleet quietens Chinese megacity,” *The Guardian*, 2018. [Online]. Available: https://www.theguardian.com/cities/2018/dec/12/silence-shenzhen-world-first-electric-bus-fleet. [Accessed: 25-Feb-2019].

[7] “Puhdasta ja hiljaista - HSL:n liikenteeseen tulee 35 uutta sähköbussia,” *HSL*, 2018. [Online]. Available: https://www.hsl.fi/uutiset/2018/puhdasta-ja-hiljaista-hsln-liikenteeseen-tulee-35-uutta-sahkobussia-16424. [Accessed: 25-Feb-2019].

[8] A. Palomaa, “Tampere valmistautuu ostamaan ensimmäiset sähköbussit,” *Yle*, 2015. [Online]. Available: http://yle.fi/uutiset/tampere_valmistautuu_ostamaan_ensimmaiset_sahkobussit/8043902. [Accessed: 25-Feb-2019].

[9] Y. Hjelt, “Sähköbussit aloittavat Turussa ensi syksynä,” *Yle*, 2016. [Online]. Available: http://yle.fi/uutiset/sahkobussit_aloittavat_turussa_ensi_syksyna/8745232. [Accessed: 25-Feb-2019].

[10] R. Wang, Y. Wu, W. Ke, S. Zhang, B. Zhou, and J. Hao, “Can propulsion and fuel diversity for the bus fleet achieve the win-win strategy of energy conservation and environmental protection?,” *Appl. Energy*, vol. 147, pp. 92–103, 2015.

[11] A. Lajunen and T. Lipman, “Lifecycle cost assessment and carbon dioxide emissions of diesel, natural gas, hybrid electric, fuel cell hybrid and electric transit buses,” *Energy*, vol. 106, pp. 329–342, 2016.

[12] J. Wang, “Barriers of scaling-up fuel cells: Cost, durability and reliability,”

Energy, vol. 80, pp. 509–521, 2015.

[13] L. Zeng, T. W. Ching, W. Li, K. T. Chau, and C. C. Chan, "Application of Electric and Hybrid Electric Buses in Macau," in *EVS29 Symposium*, 2016, pp. 1–10.

[14] B. Zhou *et al.*, "Real-world performance of battery electric buses and their life-cycle benefits with respect to energy consumption and carbon dioxide emissions," *Energy*, vol. 96, pp. 603–613, 2016.

[15] T. Sourander, "Kaupunkibussien kevytrakennetekniikka," Aalto University, 2013.

[16] D. Göhlich, T. A. Ly, A. Kunith, and D. Jefferies, "Economic assessment of different air-conditioning and heating systems for electric city buses based on comprehensive energetic simulations," *World Electr. Veh. J.*, vol. 7, no. 3, pp. 398–406, 2015.

[17] Q. Peng and Q. Du, "Progress in heat pump air conditioning systems for electric vehicles-A review," *Energies*, vol. 9, no. 4, 2016.

[18] M. André, "The ARTEMIS European driving cycles for measuring car pollutant emissions," *Sci. Total Environ.*, vol. 334–335, pp. 73–84, 2004.

[19] Z. Dai, D. Niemeier, and D. Eisinger, "Driving cycles: a new cycle-building method that better represents real-world emissions," 2008.

[20] T. Austin, F. DiGenova, T. Carlson, R. Joy, and K. Gianolini, "Characterization of driving patterns and emissions from light-duty vehicles in California. Final Report," Sacramento, California, USA, 1993.

[21] S. H. Kamble, T. V. Mathew, and G. K. Sharma, "Development of real-world driving cycle: Case study of Pune, India," *Transp. Res. Part D Transp. Environ.*, vol. 14, no. 2, pp. 132–140, 2009.

[22] W. T. Hung, H. Y. Tong, C. P. Lee, K. Ha, and L. Y. Pao, "Development of a practical driving cycle construction methodology: A case study in Hong Kong," *Transp. Res. Part D Transp. Environ.*, vol. 12, no. 2, pp. 115–128, 2007.

[23] K. S. Nesamani and K. P. Subramanian, "Development of a driving cycle for intra-city buses in Chennai, India," *Atmos. Environ.*, vol. 45, no. 31, pp. 5469–5476, 2011.

[24] J. Lai, L. Yu, G. Song, P. Guo, and X. Chen, "Development of City-Specific Driving Cycles for Transit Buses Based on VSP Distributions: Case of Beijing," *J. Transp. Eng.*, vol. 139, no. 7, pp. 749–757, 2013.

[25] S. H. Ho, Y. D. Wong, and V. W. C. Chang, "Developing Singapore Driving Cycle for passenger cars to estimate fuel consumption and vehicular emissions," *Atmos. Environ.*, vol. 97, pp. 353–362, 2014.

[26] T. R. Carlson and T. C. Austin, "Development of Speed Correction Cycles," Sacramento, California, USA, 1997.

[27] R. Zito and F. Primerano, "Drive cycle development methodology and results," Adelaide, Australia, 2005.

[28] M. André, A. J. Hickman, D. Hassel, and R. Joumard, "Driving Cycles for Emission Measurements Under European Conditions," *SAE Tech. Pap.*, 1995.

[29] F. Guo and F. Zhang, "A study of driving cycle for electric cars on Beijing urban

and suburban roads," in *2016 IEEE International Conference on Power and Renewable Energy, ICPRE 2016*, 2016, pp. 319–322.

[30] M. Peng, X. Liu, and Q. Lin, "Construction of Engine Emission Test Driving Cycle of City Transit Buses," in *SAE 2015 Commercial Vehicle Engineering Congress*, 2015.

[31] S. Ou and Y. Zhou, "Development of Hybrid City Bus's Driving Cycle," in *2011 International Conference on Electric Information and Control Engineering (ICEICE)*, 2011.

[32] B. Zhang, X. Gao, X. Xiong, X. Wang, and H. Yang, "Development of the driving cycle for Dalian city," in *Proceedings - 8th International Conference on Future Generation Communication and Networking, FGCN 2014*, 2014, pp. 60–63.

[33] J. Zhu, Q. Shi, and J. Zhou, "The city bus driving cycle construction," in *2011 2nd International Conference on Mechanic Automation and Control Engineering, MACE 2011 - Proceedings*, 2011, pp. 2687–2690.

[34] L. Berzi, M. Delogu, and M. Pierini, "Development of driving cycles for electric vehicles in the context of the city of Florence," *Transp. Res. Part D Transp. Environ.*, vol. 47, pp. 299–322, 2016.

[35] Z. Jing, G. Wang, S. Zhang, and C. Qiu, "Building Tianjin driving cycle based on linear discriminant analysis," *Transp. Res. Part D Transp. Environ.*, vol. 53, pp. 78–87, 2017.

[36] E. Silvas, K. Hereijgers, H. Peng, T. Hofman, and M. Steinbuch, "Synthesis of Realistic Driving Cycles with High Accuracy and Computational Speed, Including Slope Information," *IEEE Trans. Veh. Technol.*, vol. 65, no. 6, pp. 4118–4128, 2016.

[37] J. Lin and D. A. Niemeier, "An exploratory analysis comparing a stochastic driving cycle to California's regulatory cycle," *Atmos. Environ.*, vol. 36, no. 38, pp. 5759–5770, 2002.

[38] J. Ally and T. Pryor, "Life cycle costing of diesel, natural gas, hybrid and hydrogen fuel cell bus systems: An Australian case study," *Energy Policy*, vol. 94, pp. 285–294, 2016.

[39] J. A. García Sánchez, J. M. López Martínez, J. Lumbreras Martín, M. N. Flores Holgado, and H. Aguilar Morales, "Impact of Spanish electricity mix, over the period 2008-2030, on the Life Cycle energy consumption and GHG emissions of Electric, Hybrid Diesel-Electric, Fuel Cell Hybrid and Diesel Bus of the Madrid Transportation System," *Energy Convers. Manag.*, vol. 74, pp. 332–343, 2013.

[40] Y. Xu, F. E. Gbologah, D. Y. Lee, H. Liu, M. O. Rodgers, and R. L. Guensler, "Assessment of alternative fuel and powertrain transit bus options using real-world operations data: Life-cycle fuel and emissions modeling," *Appl. Energy*, vol. 154, pp. 143–159, 2015.

[41] G. Correa, P. Muñoz, T. Falaguerra, and C. R. Rodriguez, "Performance comparison of conventional, hybrid, hydrogen and electric urban buses using well to wheel analysis," *Energy*, vol. 141, pp. 537–549, 2017.

[42] T. Ercan, Y. Zhao, O. Tatari, and J. A. Pazour, "Optimization of transit bus fleet's life cycle assessment impacts with alternative fuel options," *Energy*, vol. 93, pp. 323–334, 2015.

[43] A. Lajunen, “Energy consumption and cost-benefit analysis of hybrid and electric city buses,” *Transp. Res. Part C Emerg. Technol.*, vol. 38, pp. 1–15, 2014.

[44] X. He *et al.*, “Energy consumption and well-to-wheels air pollutant emissions of battery electric buses under complex operating conditions and implications on fleet electrification,” *J. Clean. Prod.*, vol. 171, pp. 714–722, 2018.

[45] J. Vepsäläinen, K. Otto, A. Lajunen, and K. Tammi, “Computationally efficient model for energy demand prediction of electric city bus in varying operating conditions,” *Energy*, vol. 169, pp. 433–443, 2018.

[46] J. Vepsäläinen, “Driving Style Comparison of City Buses: Electric vs. Diesel,” in *2017 IEEE Vehicle Power and Propulsion Conference, VPPC 2017*, 2017.

[47] A. Lajunen and K. Tammi, “Energy consumption and carbon dioxide emission analysis for electric city buses,” in *EVS29 Symposium*, 2016, pp. 1–12.

[48] F. Bottiglione, T. Contursi, A. Gentile, and G. Mantriota, “The Fuel Economy of Hybrid Buses: The Role of Ancillaries in Real Urban Driving,” *Energies*, vol. 7, no. 7, pp. 4202–4220, 2014.

[49] I. S. Suh, M. Lee, J. Kim, S. T. Oh, and J. P. Won, “Design and experimental analysis of an efficient HVAC (heating, ventilation, air-conditioning) system on an electric bus with dynamic on-road wireless charging,” *Energy*, vol. 81, pp. 262–273, 2015.

[50] Z. Gao *et al.*, “Battery capacity and recharging needs for electric buses in city transit service,” *Energy*, vol. 122, pp. 588–600, 2017.

[51] A. Kontou and J. Miles, “Electric Buses: Lessons to be Learnt from the Milton Keynes Demonstration Project,” *Procedia Eng.*, vol. 118, pp. 1137–1144, 2015.

[52] J. Vepsäläinen, A. Ritari, A. Lajunen, K. Kivekäs, and K. Tammi, “Energy Uncertainty Analysis of Electric Buses,” *Energies*, vol. 11, no. 12, p. 3267, 2018.

[53] R. Prohaska, K. Kelly, and L. Eudy, “Fast charge battery electric transit bus in-use fleet evaluation,” in *2016 IEEE Transportation Electrification Conference and Expo, ITEC 2016*, 2016, pp. 1–6.

[54] A. Lajunen, “Lifecycle costs and charging requirements of electric buses with different charging methods,” *J. Clean. Prod.*, vol. 172, pp. 56–67, 2018.

[55] Q. Cheng, L. Nouveliere, and O. Orfila, “A new eco-driving assistance system for a light vehicle: Energy management and speed optimization,” in *IEEE Intelligent Vehicles Symposium, Proceedings*, 2013, no. June, pp. 1434–1439.

[56] F. Mensing, E. Bideaux, R. Trigui, and H. Tattegrain, “Trajectory optimization for eco-driving taking into account traffic constraints,” *Transp. Res. Part D Transp. Environ.*, vol. 18, no. 1, pp. 55–61, 2013.

[57] F. Mensing, E. Bideaux, R. Trigui, J. Ribet, and B. Jeanneret, “Eco-driving: An economic or ecologic driving style?,” *Transp. Res. Part C Emerg. Technol.*, vol. 38, pp. 110–121, 2014.

[58] A. Lajunen, “Energy-optimal velocity profiles for electric city buses,” in *IEEE International Conference on Automation Science and Engineering*, 2013, pp. 886–891.

[59] H. Lim, W. Su, and C. C. Mi, “Distance-Based Ecological Driving Scheme Using

a Two-Stage Hierarchy for Long-Term Optimization and Short-Term Adaptation," *IEEE Trans. Veh. Technol.*, vol. 66, no. 3, pp. 1940–1949, 2017.

[60] E. Ozatay *et al.*, "Cloud-based velocity profile optimization for everyday driving: A dynamic-programming-based solution," *IEEE Trans. Intell. Transp. Syst.*, vol. 15, no. 6, pp. 2491–2505, 2014.

[61] V.-D. Doan, H. Fujimoto, S. Member Takafumi Koseki, T. Yasuda, M. Hiroyuki Kishi, and T. Fujita, "Iterative Dynamic Programming for Optimal Control Problem with Isoperimetric Constraint and Its Application to Optimal Eco-driving Control of Electric Vehicle," *IEEJ J. Ind. Appl.*, vol. 7, no. 1, pp. 80–92, 2018.

[62] M. A. S. Kamal, J. I. Imura, T. Hayakawa, A. Ohata, and K. Aihara, "Smart driving of a vehicle using model predictive control for improving traffic flow," *IEEE Trans. Intell. Transp. Syst.*, vol. 15, no. 2, pp. 878–888, 2014.

[63] B. Ren, H. Zhao, W. Deng, and H. Chen, "Model predictive control allocation for stability improvement of four-wheel drive electric vehicles in critical driving condition," *IET Control Theory Appl.*, vol. 9, no. 18, pp. 2688–2696, 2015.

[64] D. Rubin and S. A. Arogeti, "Vehicle yaw stability control using active limited-slip differential via model predictive control methods," *Veh. Syst. Dyn.*, vol. 53, no. 9, pp. 1315–1330, 2015.

[65] X. Zeng and J. Wang, "A Parallel Hybrid Electric Vehicle Energy Management Strategy Using Stochastic Model Predictive Control With Road Grade Preview," *IEEE Trans. Control Syst. Technol.*, vol. 23, no. 6, pp. 2416–2423, 2015.

[66] M. A. Abbas, R. Milman, and J. M. Eklund, "Obstacle Avoidance in Real Time with Nonlinear Model Predictive Control of Autonomous Vehicles," *Can. J. Electr. Comput. Eng.*, vol. 40, no. 1, pp. 12–22, 2017.

[67] J. Ji, A. Khajepour, W. W. Melek, and Y. Huang, "Path planning and tracking for vehicle collision avoidance based on model predictive control with multiconstraints," *IEEE Trans. Veh. Technol.*, vol. 66, no. 2, pp. 952–964, 2017.

[68] J. Lopez-Sanz *et al.*, "Nonlinear model predictive control for thermal management in plug-in hybrid electric vehicles," *IEEE Trans. Veh. Technol.*, vol. 66, no. 5, pp. 3632–3644, 2017.

[69] R. Wang, G. Xiao, and P. Wang, "Hybrid Centralized-Decentralized (HCD) Charging Control of Electric Vehicles," *IEEE Trans. Veh. Technol.*, vol. 66, no. 8, pp. 6728–6741, 2017.

[70] C. Xiang, F. Ding, W. Wang, and W. He, "Energy management of a dual-mode power-split hybrid electric vehicle based on velocity prediction and nonlinear model predictive control," *Appl. Energy*, vol. 189, pp. 640–653, 2017.

[71] S. Zhang, R. Xiong, and F. Sun, "Model predictive control for power management in a plug-in hybrid electric vehicle with a hybrid energy storage system," *Appl. Energy*, vol. 185, pp. 1654–1662, 2017.

[72] J. Backas and R. Ghabcheloo, "Nonlinear model predictive energy management of hydrostatic drive transmissions," *Proc. Inst. Mech. Eng. Part I J. Syst. Control Eng.*, vol. 233, no. 3, pp. 335–347, 2019.

[73] M. A. S. Kamal, M. Mukai, J. Murata, and T. Kawabe, "On board eco-driving system for varying road-traffic environments using model predictive control,"

in *Proceedings of the IEEE International Conference on Control Applications*, 2010, no. October, pp. 1636–1641.

[74] M. Held, O. Flärdh, and J. Mårtensson, "Optimal Speed Control of a Heavy-Duty Vehicle in Urban Driving," *IEEE Trans. Intell. Transp. Syst.*, pp. 1–12, 2018.

[75] S. Zhang, Y. Luo, K. Li, and V. Li, "Real-Time Energy-Efficient Control for Fully Electric Vehicles Based on an Explicit Model Predictive Control Method," *IEEE Trans. Veh. Technol.*, vol. 67, no. 6, pp. 4693–4701, 2018.

[76] Argonne National Laboratory, "Autonomie," 2018. [Online]. Available: https://www.autonomie.net/expertise/Autonomie.html. [Accessed: 13-Feb-2018].

[77] Volvo Bus Corporation, "Volvo 7900 Hybrid Specifikationer," 2019. [Online]. Available: https://www.volvobuses.se/sv-se/our-offering/buses/volvo-7900-hybrid/specifications.html. [Accessed: 19-Mar-2019].

[78] Volvo Bus Corporation, "Volvo 7900 Electric Specifikationer," 2019. [Online]. Available: https://www.volvobuses.se/sv-se/our-offering/buses/volvo-7900-electric/specifications.html. [Accessed: 19-Mar-2019].

[79] Volvo Bus Corporation, "Volvo 7900 Range brochure." 2011.

[80] "Xcelsior Specs Sheet," *New Flyer Industries*, 2017. [Online]. Available: https://www.newflyer.com/site-content/uploads/2017/09/729-NFL-Xcelsior-Final.pdf. [Accessed: 05-Apr-2019].

[81] L. Eudy and M. Post, "Zero Emission Bay Area (ZEBA) Fuel Cell Bus Demonstration Results : Fourth Report Zero Emission Bay Area (ZEBA) Fuel Cell Bus Demonstration Results : Fourth Report," Denver, Colorado, USA, 2015.

[82] Linkker, "Technology," 2019. [Online]. Available: http://www.linkkerbus.com/technology/. [Accessed: 19-Mar-2019].

[83] W.-H. Hucho *et al.*, *Aerodynamics of Road Vehicles: From Fluid Mechanics to Vehicle Engineering*, 1st ed. Cambridge, UK: Elsevier, 1987.

[84] "Rolling Resistance and Rolling Noise Limits for Truck and Bus Tires according to UN Regulation 117," *Continental Tires*, 2019. [Online]. Available: https://www.continental-tires.com/transport/knowhow/un-regulation-117. [Accessed: 19-Mar-2019].

[85] T. Halmeaho *et al.*, "Experimental validation of electric bus powertrain model under city driving cycles," *IET Electr. Syst. Transp.*, vol. 7, no. 1, pp. 74–83, 2016.

[86] M. Kim, D. Jung, and K. Min, "Optimal torque distribution strategy for dual traction motors in a series hybrid electric intra-city bus," *Int. J. Heavy Veh. Syst.*, vol. 24, no. 1, pp. 18–44, 2017.

[87] A. Lajunen and A. Kalttonen, "Investigation of Thermal Energy Losses in the Powertrain of an Electric City Bus," in *Transportation Electrification Conference and Expo (ITEC), 2015 IEEE*, 2015.

[88] J. Vepsäläinen, K. Kivekäs, K. Otto, and K. Tammi, "Development and Validation of Energy Demand Uncertainty Model for Electric City Buses," *Transp. Res. Part D Transp. Environ.*, vol. 63, pp. 347–361, 2018.

[89] M. Hinkkanen, “Electric Drives - lecture notes.” Aalto University, Espoo, Finland, 2016.

[90] Federal Transit Administration, “Bus Testing: Calculation of Average Passenger Weight and Test Vehicle Weight,” 2012. [Online]. Available: https://www.federalregister.gov/documents/2012/12/14/2012-30184/bus-testing-calculation-of-average-passenger-weight-and-test-vehicle-weight. [Accessed: 01-Apr-2019].

[91] J. Anttila, “Uncertainty in electric bus driving cycles,” Aalto University, 2016.

[92] L. L. Hoberock, “A survey of longitudinal acceleration comfort studies in ground transportation vehicles,” *J. Dyn. Syst.*, vol. 99, no. 2, pp. 76–84, 1977.

[93] X. Karekla and N. Tyler, “Reducing non-collision injuries aboard buses: Passenger balance whilst walking on the lower deck,” *Saf. Sci.*, vol. 105, no. February, pp. 128–133, 2018.

[94] C. Zaiontz, “Basic Concepts of Correlation,” *Real Statistics Using Excel*, 2019. [Online]. Available: http://www.real-statistics.com/correlation/basic-concepts-correlation/. [Accessed: 03-Apr-2019].

[95] F. Cannavó, “Sensitivity analysis for volcanic source modeling quality assessment and model selection,” *Comput. Geosci.*, vol. 44, pp. 52–59, 2012.

[96] C. Xu and G. Z. Gertner, “Uncertainty and sensitivity analysis for models with correlated parameters,” *Reliab. Eng. Syst. Saf.*, vol. 93, no. 10, pp. 1563–1573, 2008.

[97] “Coefficient of Determination (R-Squared),” *MathWorks*, 2019. [Online]. Available: https://se.mathworks.com/help/stats/coefficient-of-determination-r-squared.html. [Accessed: 03-Apr-2019].

Aalto-DD 133/2019

ISBN 978-952-60-8647-7 (printed)
ISBN 978-952-60-8648-4 (pdf)
ISSN 1799-4934 (printed)
ISSN 1799-4942 (pdf)

Aalto University
School of Engineering
Department of Mechanical Engineering
www.aalto.fi

BUSINESS + ECONOMY

ART + DESIGN + ARCHITECTURE

SCIENCE + TECHNOLOGY

CROSSOVER

DOCTORAL DISSERTATIONS